CATALYTIC AND SURFACE OXIDATION PROCESSES ON TRANSITION METAL SURFACES

Sampsa Jaatinen

Laboratory of Physics
Helsinki University of Technology

Fysiikan laboratorio
Teknillinen korkeakoulu

DISSERTATION 146 (2007)

CATALYTIC AND SURFACE OXIDATION PROCESSES ON TRANSITION METAL SURFACES

Sampsa Jaatinen

Laboratory of Physics
Helsinki University of Technology
Espoo, Finland

Dissertation for the degree of Doctor of Science in Technology to be presented with due permission of the Department of Engineering Physics and Mathematics, Helsinki University of Technology for public examination and debate in Auditorium E at Helsinki University of Technology (Espoo, Finland) on the 23rd of March, 2007, at 12 o'clock noon.

Dissertations of Laboratory of Physics, Helsinki University of Technology
ISSN 1455-1802

Dissertation 146 (2007):
Sampsa Jaatinen: Catalytic and surface oxidation processes on transition metal surfaces
ISBN 978-951-22-8685-0 (print)
ISBN 978-951-22-8686-7 (electronic)

Multiprint Oy / Otamedia
Espoo 2007

Abstract

Transition metals are technologically important catalytic materials. The transition metal catalysts are used for example in petroleum and fertilizer industry. In the car industry the catalytic materials are used in the catalytic converters. Because of the industrial importance the catalytic metals have been widely studied throughout the past decades. Nonetheless, the oxidation mechanisms of small molecules and the effect of alloying to catalytic properties of metals are not fully understood.

In this thesis the catalytic effect of a palladium-silver alloy on the oxidation of a carbon monoxide molecule is studied with a computational approach. With *ab initio* methods we have been able to investigate the underlying microscopic processes of the oxidation. We have studied how the Pd atoms introduced to an Ag surface change the catalytic properties of the material. It has been seen that the Pd atoms enhance the dissociation of the O_2 molecules, strengthen the binding of the CO molecules and lower the reaction barrier of the oxidation process.

In addition to the oxidation of the carbon monoxide, the oxidation of copper surfaces has been studied. Copper is widely used for example in construction, water pipes and other large scale facilities. On the other hand, it is used in a microscopic level in electronics as s conductor and the copper oxide as an insulator. In all of these examples the oxidation of copper plays a crucial role and it also possesses a great commercial value. In some applications the oxidation is an unwanted phenomenon, whereas in some other applications the properties of grown oxide are exploited. The oxidation of copper surfaces is also scientifically interesting since the oxygen is known to induce a reconstruction of the surface. The reconstruction structure has intensively been studied, but still the initial steps of the oxidation and reconstruction are not completely explained.

In this thesis, the reconstruction and the growth of the oxide layer on Cu(100) are studied with a multi-scale modeling involving both the atomistic electronic structure calculations and the larger scale statistical simulations. With the combined modeling we have been able to reproduce and further explain the structures observed in the experiments. We have shown that the dissociation and diffusion of oxygen is more rapid on the clean Cu(100) surface than on the reconstructed parts of the surface. The Cu adatoms form rapidly stable (100) islands and O adatoms form separate $c(2 \times 2)$ domains.

Preface

This thesis has been prepared in the Laboratory of Physics at the Helsinki University of Technology during the years 2002-2006. I wish to thank Academy Prof. Risto Nieminen for the opportunity to work in the Computational Nanoscience group (COMP) and for being the supervisor of this work. My instructor, Doc. Petri Salo I wish to thank for his guidance and efforts. To Dr. Marko Rusanen I am grateful of the instructions and guidance in the fields of Monte Carlo and statistical physics. My former instructor Prof. Matti Alatalo and colleagues Antti Puisto and Mika Jahma I wish to thank for the collaboration and fruitful discussions. Dr. Simo Särkä I wish to than for his valuable help with the Monte Carlo method and stochastics. I thank all the personnel at the Laboratory of Physics, friends at work and their company during coffee breaks. I acknowledge the computing resources of CSC–Scientific Computing Ltd and the scholarship granted by the Finnish Academy of Science and Letters.

Finally, I wish to thank my parents, brothers and especially Taru, who never failed me.

Espoo, March 2007

Sampsa Jaatinen

Contents

List of Publications

This thesis consists of an overview and the following publications:

I Jaatinen, S., Salo, P., Alatalo, M., Kulmala, V., and Kokko, K., Structure and reactivity of Pd doped Ag surfaces. *Surface Science*, 529:403, 2003.

II Jaatinen, S., Salo, P., Alatalo, M., and Kokko, K., Reactivity of Pd doped Ag surfaces. *Vacuum*, 74:169, 2004.

III Jaatinen, S., Salo, P., Alatalo, M., and Kokko, K., Effect of the electronic structure on CO oxidation on Pd doped Ag(111). *Surface Science*, 566-568:1063, 2004.

IV Alatalo, M., Jaatinen, S., Salo, P., and Laasonen, K., Oxygen adsorption on Cu(100): First-principles pseudopotential calculations. *Physical Review B*, 70:245417, 2004.

V Jaatinen, S., Blomqvist, J., Salo, P., Puisto, A., Alatalo, M., Hirsimäki, M., Ahonen, M., and Valden, M., Adsorption and diffusion dynamics of atomic and molecular oxygen on reconstructed Cu(100). *Physical Review B*, 75:075402, 2007.

VI Jaatinen, S., Rusanen, M., and Salo, P., A multi-scale Monte Carlo study of oxide structures on the Cu(100) surface. *Surface Science*, in print, 2007.

The author has had an active role in all stages of the research. He has been involved in plannig and conducting the *ab initio* calculations and interpreting the results. He has conducted all the calculations in Paper I and all, expect the results for Pd surfaces, in Papers II and III. In Paper IV he has made the diffusion calculations presented. In Paper V the author have conducted all the molecular adsorption and atomic diffusion calculations. The author has written the Monte Carlo code used in the simulations of Paper VI and conducted all the simulations. He has written the manuscript VI, the first draft of publications II and V and contributed actively on writing the other publications.

1 Introduction

Because of its economical relevance, catalysis is an intensively studied field of applied chemistry and engineering. Most of the industrial chemical processes are catalytic, for example economically vastly important processes such as cracking the long hydrocarbons in petroleum into smaller hydrocarbons, primarily into gasoline, the synthesization of ammonia used in fertilizers, oxidation of the exhaust carbon monoxide (CO) in the catalytic converter of cars and so on. A great number of the most effective catalysts are metallic, and more precisely, transition metals [1]. This gives the transition metal catalysts a great technological meaning which has motivated a wide investigation of the catalysis and transition metal surfaces [2]. Our focus has been in oxidation, because of the crucial role it has in several industrially essential processes and applications. Not only in the sense of unwanted corrosion but as an effective part in applications including gate oxides in electronics, forming passivation layers and in several catalytic reactions. Indeed, it has been found recently that the catalytically active part of the surface can be in fact the metal oxide and not the metal itself [3].

In this thesis two different kind of oxidation processes are studied. First we discuss the CO oxidation and the catalytic effect of palladium silver alloys on the process. The poisonous CO-gas is a typical exhaust gas in burning and combustion processes. A common example is exhaust gases of cars. The CO is also a strong greenhouse gas and therefore it is important to reduce its production with the catalysis technology.

There are several effective catalytic materials for CO oxidation, for example Pd, Pt and Rh. The primary interest for enhancing the properties of silver rather than simply to use pure palladium, or such rises from the most practical reasons. Raw silver costs roughly 13 USD/oz., in the raw materials exchange, whereas palladium costs 320 USD/oz., platinum 1200 USD/oz. and rhodium 4800 USD/oz [4]. It is evident that these differences in prices will motivate the usage of silver even if another metal might make a more robust catalyst for a desired purpose. Wouda *et al.* [5] have shown that the reactivity of Ag surfaces towards the CO oxidation can be modified by alloying the Ag surfaces. To study this further we have investigated the structure and reactivity of a Pd-Ag alloy with quantum mechanical first principles (*ab initio*) methods. With these methods we are able to study the electronic and structural effects that alloying has on surfaces and how this alters the catalytic properties of the material.

The second viewpoint is the oxidation of the surface itself. The chosen problem is the oxidation of the Cu(100) surface. Copper surfaces are common and they possess some interesting properties such as formation of different kind of oxygen domains and oxygen induced surface reconstruction. The macroscopic aspects of the oxidation are well known but it is not completely understood how it proceeds on the atomic scale. Copper is also a widely used material having a broad range of applications varying from very big scale usage e.g. in water pipes and building construction to micro scale usage as an electric conductor in electronics. The oxidation problem is in common on all of these scales and in all of these applications.

It is of a great commercial and also scientific significance to understand and to be able to control the oxidation. We already know some of the effects of the oxidation and how to prevent it or how to live with it. If we understood the very microscopic features of the oxidation better, we could also better control the phenomenon and use it to our advantage. To gain deeper insight into these processes, it is crucial to know the oxidation mechanisms at the nanometer scale.

There are several experimental [1, 6, 7, 8] and computational studies [9, 10, 11, 12] on oxygen behavior on Cu(100) surface and on the epitaxial growth of copper [13]. To extend these studies we have performed multi-scale modeling by applying the *ab initio* electronic structure calculations to study the energetics of very elementary atomic scale processes of Cu and O ad-atom movements on the Cu(100) surface. We have used this energetics to conduct statistical Monte Carlo simulations which give us an opportunity to see the emerging of structures on a larger scale than what we are able to simulate with the *ab initio* methods alone. This allows us to study also the temperature dependence of stable and metastable structures, growth of islands and the self-assembling of other structures. This might be the key in understanding the early stages of macroscopic oxidation.

In the multi-scale modeling the model on a larger scale is based on the observations and results of the smaller scale model. For example in our case the statistical model is based on the energetics obtained with the electronic structure calculations on an atomic scale. This kind of chain of models and coarse graining can give a new insight into how the phenomena and structures on a larger scale emerge from the very elemental principles.

2 Oxidation

We have studied two different kind of oxidation processes. First we study processes of adsorbate oxidation and especially the oxidation of CO. These kind of oxidation processes are commonly catalyzed by transition metals where the reaction takes place on the surface of the catalytic material. Whether the surface itself get oxidized, depends on the reaction type. For example on the Pd(100) catalyzed CO oxidation, a thin oxide layer is formed and sustained in the steady state [14]. In the real conditions there may also occur oscillations between a clean metal and the oxide surface [14].

The second subject that we have studied is the oxidation of the surface itself. The oxidation may dramatically affect the properties of the surface. In some cases the catalytic properties can be changed since the electronic structure of the oxidized surfaces is totally different from that of the clean ones. It has been shown that on the case of Ru catalysts the catalytic surface is indeed a RuO_2 oxide surface [3, 15]. Also the mechanical and electric properties of the surface can be changed and the material may lose its strength and hardness. The corrosion resistance of iron or steel can be achieved with a passivation layer of oxidized chromium Cr_2O_3 [16]. Similarly the acid resistance of steels is based on a pre-oxidized passivation layer. On some surfaces this kind of passivation layer does not form and instead, oxygen can force the surface to reconstruct as in the case of Cu(100) [17] or the oxygen slowly diffuses deeper into the metal causing the oxide layer to grow thicker and thicker.

2.1 Transition metals

Considering catalysts there are a few interesting notions. A great number of solid catalytic materials are metallic [18]. And more precisely, almost all of the metal catalysts are transition metals and the catalytic behavior is clearly associated with the presence of the *d*-orbital [18].

The elements in the periodic table groups IIIB-IIB are commonly called transition metals. There is an alternative and more strict definition according to which transition metals are materials with an incomplete d sub-shell, bordering out the elements with the d^{10} configuration. I will not use this definition because in some cases the filling of the states is different for isolated atoms and for atoms in bulk. The bulk transition metals are formed

by a strong hybridization among the s orbitals of the metal atoms. These s-bands are quite broad in energy ≈ 20 eV whereas the p and d orbitals are narrower being ≈ 4 eV in energy and they interact more weakly with the other atoms in a bulk metal [18]. As the s-band is broad in the energy it typically overlaps with the narrower d-band. The d-band being narrow and having high density of states may have some of its states unfilled, which is the case for example for Ni and for bulk Cu. The atomic Cu has a full d-band [19]. The unfilled states are called holes in the d-band. The relative strength of metal bonding also depends on the filling of the d-band, since empty and filled orbitals cannot contribute to the bonding because of the lack of the hybridization [18]. We have studied the propertied of Pd with $4d^{10}5s^0$, Ag with $4d^{10}5s^1$ and Cu with $3d^{10}4s^1$ electronic configurations [17]. For catalysis and oxidation the possible strong surface state of the electronic structure is relevant. Two different transition metals combined may have their d-band and reactivity greatly changed. For example, even small amounts of roughly 5% of Al alloyed to a Cu(100) surface greatly enhances the reactivity of the surface to the oxidation [20]. In this thesis the effect of alloying on the electronic structure and reactivity is studied in terms of PdAg compounds and the catalyzed oxidation of the CO into CO_2 molecules. The surface oxidation of copper (100) surface is studied together with the oxygen induced $(2\sqrt{2} \times \sqrt{2})R45°$-O reconstruction on Cu(100).

2.2 Oxidation and Catalysis

Our interest has been on the oxidation of toxic CO molecules into less harmful CO_2. This is a simple oxidation problem, which has a relatively slow reaction rate in a gaseous mixture. It is known that transition metals such as platinum, palladium and ruthenium are capable of speeding up the oxidation process significantly [14, 21].

Considering the surface catalysis there are two different basic processes. In the Eley-Rideal process, one of the reaction compounds is first adsorbed on the surface and it interacts with another compound in the gaseous phase. After interaction the newly formed molecule desorbs, see Fig. 1 [1]. The other major type is the Langmuir-Hinshelwood process, where both of the reaction compounds are first adsorbed on the surface where they diffuse to each other's vicinity and react. After the reaction the formed compound again desorbs into the gaseous phase, see Fig. 2 [1].

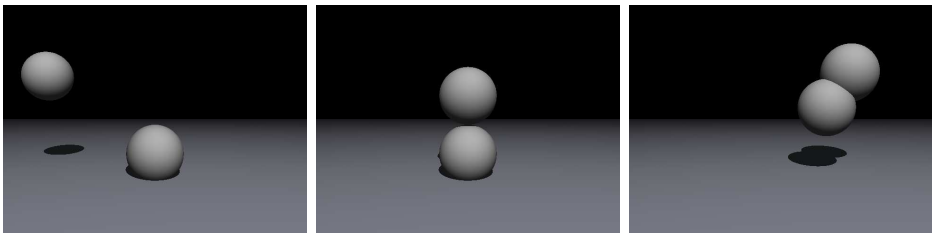

Figure 1: Eley-Rideal process

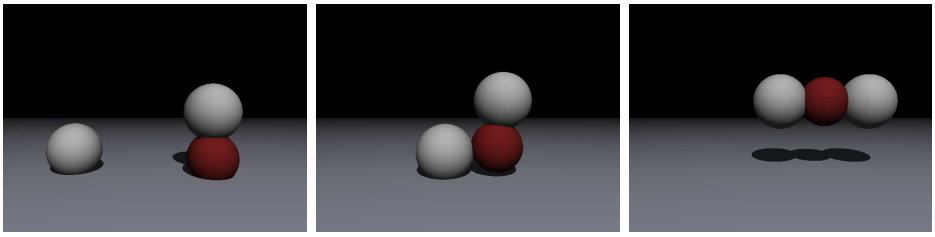

Figure 2: Langmuir-Hinshelwood process

The oxidation processes have been widely studied along last decades. Especially the proven strength of *ab initio* methods in the catalysis studies has emerged a wide range of investigations [22]. The catalytic oxidation of CO e.g. on Pt and Ru surfaces is one of the most widely studied processes because of its supposed simplicity and prevalence. The Ru(0001) surface is seen to speed up the oxidation of CO especially at high temperatures and pressures [23]. Ru(0001) dissociates the O_2 efficiently but, on the other hand, it binds O and CO relative strongly which disfavors the oxidation reaction [24]. In ultra high vacuum conditions ruthenium is known to be a poor catalyst. In contrast, Pt, Pd, Ir, and Rh do not work best on the highest O coverages [24]. For example on the widely studied Pt(111) the oxidation is accelerated most when the coverages of O and CO on the surface are equal, i.e. in stoichiometric proportions [25]. The behavior of the Ru(0001) surfaces is related to the observation by Over *et al.* [3] that on high O exposures the reactive surface becomes to be the RuO_2 oxide surface and not the clean Ru(0001) surface. In the industrially important conditions the Ru seems to be the most efficient catalytic material for oxidizing CO. The oxidation of CO on elemental Ag surfaces is known to be weak, but the reactivity of Ag surfaces can be enhanced by introducing small amounts of

Pd atoms on the surface [5].

The oxidation barrier on transition metal surfaces is within a good approximation dominated by the strength of the bond between the O atoms and the surface [26]. But for the real oxidation processes also the dissociation of O_2 and the diffusion of adsorbates on the surface are important. Altogether, there are plenty of studies on the catalysis of CO oxidation on elemental surfaces, but hetero-structure surfaces and the effect of alloying have not been systematically studied at equal extent.

2.3 Surface oxidation

The catalysis and other properties of the surface are very condition dependent. The temperature of the surface, defects and impurities etc. are known to have an effect on the behavior of the surface. The interaction between atoms and small molecules such as carbon, nitrogen or oxygen and the surface is usually determined by the interplay between the p-band of the molecule and the d-band of the transition metal surface [27].

In the weak physisorption binding, the molecule is bound to the surface due to the van der Waals forces, meaning that the bonding is due to the induced dipole moment of nonpolar adsorbate interacting with its own image charge [28]. In contrast, the chemisorption is considered as a "real bonding" between the adsorbate and the surface. The local density of states (LDOS) at the Fermi-level can be associated with the reactivity of the surface as in chemisorption there is considerable hybridization of the electronic orbitals of the surface atoms and the adsorbate atom or molecule. Furthermore, B. Hammer *et al.* [29] have shown that the strength of the interaction can be characterized by the center of the d-band of the surface atom. This is because the shift in the d-orbitals of the surface causes a relative shifting of the bonding and anti-bonding levels between the surface and the adsorbate, see Fig. 3 for a schematic representation.

In a real oxidation process, one of the crucial steps is the dissociation of O_2 molecules. The same goes for the oxidation of CO into CO_2, several other molecular oxidation problems and the oxidation of the surfaces. In the oxidation, a single O atom is most often needed as the O_2 molecule is energetically stable because of the double bond. Of course for the reaction $CO \rightarrow CO_2$ atomic oxygen is needed. The dissociation, diffusion, and reac-

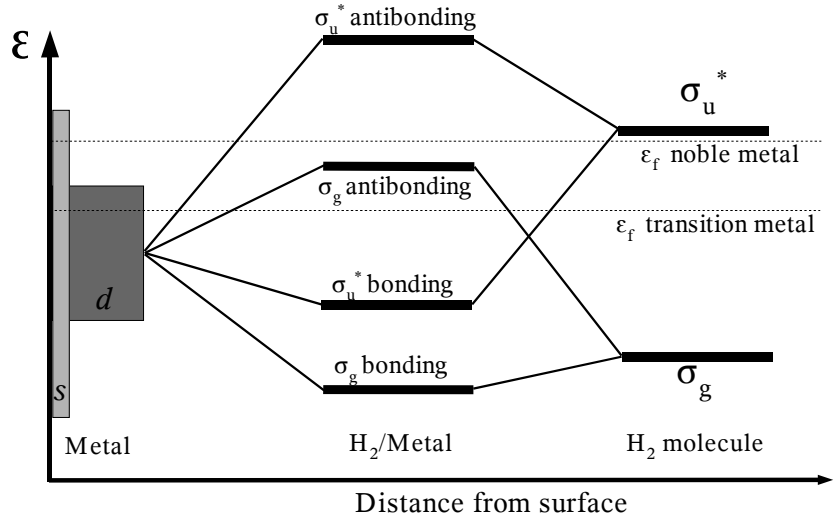

Figure 3: A schematic picture of the bonding of H_2 molecule on metal and the formation of bonding and anti-bonding levels. Transition and noble metals have a relatively narrow *d*-band. For a transition metal the Fermi-level ϵ_f is inside the *d*-band and for a noble metal above the band [28].

tion rates depend on the surface and it is not straightforward to say which is the rate limiting step.

There are a few possible ways to study the dissociation energies of molecules in the vicinity of a surface. One of the elementary ways is quantum molecular dynamics which is a robust method but also computationally demanding. A simpler way is to calculate the energy of the system with different adsorbate-surface distances and with different adsorbate bond lengths. This way one forms a two dimensional cut from the real potential energy surface (PES), which may give a good approximation and insight into the dissociation energetics. The surface defects, steps and impurities are known to have a significant effect on the dissociation [28], which is also related to the interest of alloying, since even a small amount of impurity atoms at the surface may dramatically alter the reactivity and mechanical properties of metal materials.

In experiments it is sometimes desirable to induce high O coverages on sur-

faces. The highest oxygen coverages are obtained with stronger oxidants than O_2, for example NO and NO_2. Oxygen molecules do not easily oxidize transition metal surfaces such as Pt, Pd and Ag because of the low dissociation rate [5, 30]. The behavior of oxidation as a function of temperature is also different between NO_2 and O_2 exposures. For example on Pd(111) surface the temperature does not have effect on the observed coverage under O_2 exposure, but after the NO_2 exposure the coverage increases strongly with elevated temperatures [30]. It seems that the dissociation of O_2 on Pd(111) is not thermally activated, but it is rather some indirect dissociation mechanism for example a precursor mediated process [30]. The case is similar to the O pre-covered Cu(100) which exhibits the same behavior and for which a precursor mediated dissociation process has been suggested. For details consider Paper **V**. The oxide structure can grow on surfaces either by layer-by-layer fashion or by island growth. Also it is possible that both of the processes are involved in the different stages of the growth. The surface oxide structure of Cu(100) grows in the layer-by-layer manner up to one monolayer (ML) of oxygen and then proceed by the growth of Cu_2O islands [7]. The first grown layer is the reconstruction layer on which the reconstruction islands begin to nucleate.

3 Density Functional Theory

The Density functional theory (DFT) has taken a solid position in computational materials science during the past decades. The DFT approach has been widely used for studying for example transition metals, semiconductors and other solid state systems. First principles calculations provide a controllable way to study the effects of alloying. The method allows us to vary the concentration, and thereby study the structural and electronic changes it imposes on materials. Using DFT methods in catalysis calculations enables us to seek accurately transition rates and reaction energetics. In this section the basic theory of DFT calculations with the related approximations is presented.

3.1 Hohenberg-Kohn theorem

The density functional theory is based on a theorem by Hohenberg and Kohn [31] which suggests that the electron density may be taken as a basic variable on which all the other physical quantities depend. The following shows the general idea how this can be done.

Let us consider a typical time-independent Hamiltonian of a many body system

$$\widehat{H} = \widehat{T} + \widehat{V} + \widehat{W}, \tag{1}$$

where the kinetic energy operator is

$$\widehat{T} = \frac{-\hbar^2}{2m} \sum_i \langle \psi_i | \nabla^2 | \psi_i \rangle. \tag{2}$$

$\widehat{W}$ represents the electron-electron interaction

$$\widehat{W} = \sum_{i,j} \langle \psi_i \psi_j | w(\vec{r}_i, \vec{r}_j) | \psi_j \psi_i \rangle \tag{3}$$

and the ionic core potential is

$$\widehat{V} = \langle \psi_i | v(\vec{r}_i) | \psi_i \rangle. \tag{4}$$

Now we define a set $\mathbf{V}$ of local one-particle potentials such that for all $\widehat{V} \in \mathbf{V}$ the solution to the problem

$$(\widehat{T} + \widehat{V} + \widehat{W})|\psi\rangle = E|\psi\rangle \tag{5}$$

gives a nondegenerate ground state energy E of the many particle problem [32]. The Schrödinger equation defines a mapping $\sigma : \mathbf{V} \to \mathbf{\Psi}$. Here $\mathbf{\Psi}$ is the set of all ground state wave functions. For all many-particle ground state wave functions $\Psi \in \mathbf{\Psi}$ one can calculate the ground state density

$$n(\vec{r}) = \langle \Psi | \widehat{n}(\vec{r}) | \Psi \rangle \tag{6}$$

with the fermion density operator $\widehat{n} \in \mathbf{N}$ as the sum of one particle densities

$$\widehat{n}(\vec{r}) = \sum_i \psi_i^*(\vec{r})\psi_i(\vec{r}). \tag{7}$$

A calculation of the ground state densities defines again a mapping $\rho : \mathbf{\Psi} \to \mathbf{N}$ from the set of ground state wave functions to the set of ground state densities.

Both of the mappings defined here are known to be bijective [32] and thus there exist inverse mappings σ^{-1} and ρ^{-1} which together define a mapping $\sigma^{-1}\rho^{-1} : \mathbf{N} \to \mathbf{V}$. This gives us a unique dependence between the ground state wave functions and the ground state densities. Thus the ground state density may be taken as a basic variable on which all the other variables depend.

The theory is valid for potentials that are "smooth enough" and may be extended to nondegenerate ground states as well [32]. The theory is based on the Schrödinger equation which guarantees that all physical densities represent some physical wave functions. It is, however, possible to define unphysical densities that cannot be represented with any potential $v(\vec{r}, \vec{r}')$ in the Schrödinger equation. Since the restriction is for unphysical potentials it will not be considered here any further. For more details see the book by Dreizler and Gross [32].

3.2 Kohn-Sham equations

The Hohenberg-Kohn theorem shows the theoretical basis for taking the density as a basic variable. The problem is how the functionals should be

formulated if one wants them on one hand to predict the physical quantities correctly and on the other hand to be as easy to be used as possible. This makes the description of the many particle system an essential problem in studying the structure of matter, since it is known that only the most simple cases may be solved analytically or even in a numerically exact way. Let us introduce the basic idea of the Kohn-Sham scheme which implements the DFT for the usage of calculating properties of condensed matter [33]. According to the Hohenberg-Kohn theorem the electronic energy is a functional of the electronic density $n(\vec{r})$ and it takes the form [33]

$$E[n(\vec{r})] = \int v(\vec{r})n(\vec{r})d\vec{r} + \frac{1}{2}\int\int \frac{n(\vec{r})n(\vec{r}\,')}{|\vec{r}-\vec{r}\,'|}d\vec{r}d\vec{r}\,' + G[n], \tag{8}$$

where $n(\vec{r})$ is the electronic density and $G[n]$ is a functional of the density. This expression gives the ground state energy for the correct density $n(\vec{r})$. The energy functional $G[n]$ may be written as

$$G[n] = T_s[n] + E_{xc}[n], \tag{9}$$

with $T_s[n]$ being the kinetic energy of a noninteracting system and $E_{xc}[n]$ giving the exchange and correlation energy of an interacting electron system, both with the same density $n(\vec{r})$. Basically the nonlocal exchange potential is defined according to the theorem by Hartree and Fock as

$$\widehat{V}_x = -\frac{1}{2}\sum_{i,j}\int\int d\vec{r}d\vec{r}\,' \frac{e^2\delta_{s_i,s_j}}{|\vec{r}-\vec{r}\,'|}\psi_i^*(\vec{r})\psi_i(\vec{r}\,')\psi_j^*(\vec{r}\,')\psi_j(\vec{r}), \tag{10}$$

where s_i and s_j refers to the spin states of corresponding electrons [19]. With the exchange energy we can also define the correlation energy which is the difference between the exact solution of the problem and the solution achieved with the Hartree-Fock (HF) approximation.

The exchange-correlation term contains quantum mechanical manybody effects. Two electrons with the same spin cannot be at the same position. In the HF approximation, the antisymmetry of the wavefunction takes into account the correlation between the positions of the electrons [28]. This is called exchange energy which is described with the exchange hole density. An electron with spin i causes depletion, or a hole, of electrons with the opposite spin in the near region. Also the electrons with the same spin may have their movement correlated. This effect is called electron correlation and it is incorporated to the exchange-correlation energy functional. The

approximation of the exchange-correlation functional is not straightforward and it will be discussed briefly later on.

Not worrying about the exact form of the energy functionals we can proceed with the formal treatment. The foundation of the Kohn-Sham scheme is based on the assumption that the exact ground state density of the interacting system equals to the ground state density of the system with local single-particle potential and the corresponding charge density [32].

For the nondegenerate ground state the density has a unique representation

$$n(\vec{r}) = \sum_{i=1}^{N} |\psi_i(\vec{r})| \tag{11}$$

which together with the one particle Schrödinger equations

$$\widehat{H}_i\psi_i = \left(\frac{-\nabla^2}{2m} + \widehat{V}_{ion}(\vec{r}) + \widehat{V}_h(\vec{r};n) + \widehat{V}_{xc}(\vec{r};n)\right)\psi_i(\vec{r}) = \epsilon_i\psi_i(\vec{r}) \tag{12}$$

are called the Kohn-Sham equations [33]. The great advantage of this model is that only the exchange and correlation functionals need approximations whereas the kinetic energy functional may be treated exactly [34]. One has to keep in mind that the functional is exact only for the noninteracting system and does not describe exactly the interacting system even if the functional itself may be treated exactly. In the Kohn-Sham scheme these equations are solved self-consistently for the charge density.

We may rewrite Eq. (12) as

$$(\widehat{T}[n] + \widehat{V}_{eff}[n])\psi_i = \epsilon_i\psi_i. \tag{13}$$

Here we call $V_{eff}[n]$ an effective potential, which consists of three terms. $\widehat{V}_{ion}$ is the ionic potential caused by the positively charged ions cores and $\widehat{V}_h$ is the Hartree electrostatic potential of the electrons

$$\widehat{V}_h = \int d\vec{r}\,' \frac{n(\vec{r}\,')}{|\vec{r} - \vec{r}\,'|}. \tag{14}$$

Generally, the third term of V_{eff}, the exchange-correlation potential $V_{xc} = \epsilon_{xc}n(\vec{r}) + n(\vec{r})\frac{\partial\epsilon_{xc}}{\partial n(\vec{r})}$ is not explicitly known. The first approximation for the exchange-correlation functional is to assume a slowly varying density, i.e.

that the local electron density is almost constant. This is the so-called local density approximation (LDA) giving the exchange-correlation energy as [33]

$$E_{xc}^{LDA} = \int n(\vec{r})\epsilon_{xc}[n(\vec{r})]d\vec{r}. \tag{15}$$

The LDA has been widely used and it gives good results especially for bulk properties. For certain cases the approximation of slowly varying charge density is not valid anymore. Especially for the valence states on metal surfaces the approximation of slowly varying density is not realistic [35]. Also for small molecules and adsorption calculations, the LDA results can deviate dramatically from the experimental results. For these purposes several types of generalized gradient approximations (GGA) have been developed. In the GGA the exchange-correlation is not only a functional of the value of the electron density but also a functional of the different kind of gradient expansions of it. In certain applications the GGA's have shown to give significantly better results for the properties of systems studied.

For example, for the dissociation energy of an O_2 molecule is experimentally observed 5.23 eV. The LDA results deviate from this value even more than 2 eV, whereas the GGA results deviate less than 1 eV, and at their best only few tenths of an eV [36]. Probably the most commonly used GGA's are the functionals developed by Perdew and Wang [37], Perdew and Becke [38, 39], Perdew, Burke and Ernzerhof [40] and revised Perdew, Burke and Ernzerhof [36].

3.3 Plane Wave Pseudo Potential Method

How easily the Kohn-Sham equations can be solved depends on the used potentials [41]. For example if we consider the electron-ion interaction as the simple Coulombic potential it diverges at the centers of ions, which is unacceptable within numerical approaches. The potential seen by an electron caused by the other electrons and ion cores may be treated within several different approximations. The chemical properties of most atoms is determined by the valence electrons [28]. By dividing the space around the atoms into core and valence region the description of chemical properties can be preserved even if the the potential inside the core region is strongly approximative, see Fig. 4. The smoothed potential inside core region requires a smaller basis set for approximating the wave functions, and thus

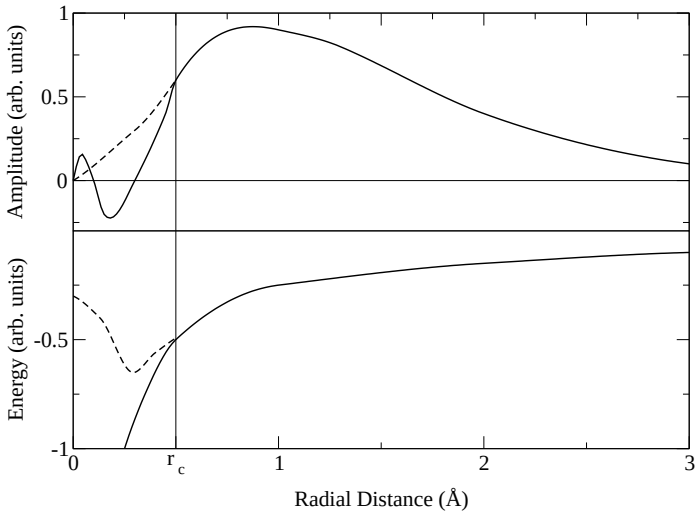

Figure 4: In the upper panel a schematic representation of the all-electron (solid line) and pseudo wave function (dashed line) and in lower panel their corresponding potentials. The core radius is illustrated with vertical line at r_c [28].

lighter computation with a suitable accuracy [41]. This has lead into the development of pseudo potentials.

In the first simulations the pseudo potential approximation together with the plane wave expansion was applied. In a plane wave basis the valence wave function ψ may be represented as a Fourier series

$$\psi_{\vec{k}n}(\vec{r}) = \sum_{k,G} \psi_{\vec{k}n}(\vec{G}) e^{i(\vec{k}+\vec{G})\cdot\vec{r}}, \tag{16}$$

where $\vec{G}$ denotes a reciprocal lattice vector and $\vec{k}$ a wave vector. If the wave function (16) is an eigenfunction of the Hamiltonian in Eq. (1) then $\psi_{\vec{k}n}(\vec{G})$ is an eigenfunction of the corresponding Hamilton operator with Fourier transformed potential and charge density terms. Furthermore, this plane wave basis may be orthogonalized in such a way that the valence plane wave of the wave vector $\vec{k}$ can be made orthogonal to the core wave functions with an equivalent $\vec{k}$ [42].

Once the atomic space is divided into the core and valence regions, the core region has effectively positive charge which possesses an attractive potential to the electrons at the valence region. Even if the attraction is quite strong, the requirement of the valence electron wave functions to be orthogonal to the core state wave functions results in a large kinetic energy of the valence states. This kinetic energy causes an effectively repulsive potential for the valence states, which may be presented as a pseudopotential constructed in the terms of the valence and core state wave functions $|\psi_v\rangle$ and $|\psi_c\rangle$ [41]. The pseudo-states are defined as

$$|\phi_v\rangle = |\psi_v\rangle + \sum_c |\psi_c\rangle\langle\psi_c|\phi_v\rangle. \tag{17}$$

Applying the Hamiltonian with the eigenfunctions $|\psi_v\rangle$ and $|\psi_c\rangle$ on Eq. (17) gives

$$\widehat{H}|\phi_v\rangle = E_v|\psi_v\rangle + \sum_c (E_c - E_v)|\psi_c\rangle\langle\psi_c|\phi_v\rangle. \tag{18}$$

From here we define a pseudo Hamiltonian

$$\widehat{H}^{ps}(E) = \widehat{H} + \sum_c (E - E_c)|\psi_c\rangle\langle\psi_c| \tag{19}$$

and according to Philips and Kleinman [43] the pseudopotential is defined as

$$\widehat{V}^{PK} = \widehat{V} + \sum_c (E - E_c)|\psi_c\rangle\langle\psi_c|. \tag{20}$$

The pseudopotential defined here is used to describe the effective potential in our many-particle systems. This is efficient because the pseudopotential is relatively weak compared to the full potential V and thus it is easier to handle. This method is known to be efficient and accurate for metals with no d or f bands in the valence region [34, 41].

The *ab initio* pseudopotentials are constructed from the atomic calculations without free parameters and they reproduce the correct wave functions in correct normalization. Hamann, Schlüter and Chiang [44] introduced the norm-conserving pseudopotentials, for which several generation schemes have been developed. A further improvement was the development of the ultra-soft pseudopotentials. D. Vanderbilt introduced a method for constructing pseudopotentials from all electron wavefunctions in a way that the general norm-conserving condition becomes unnecessary [45]. Without the norm-conservation constraint it is possible to choose the cutoff radius beyond the radial wavefunction maximum that makes the core region even smoother and potentials more capable of modeling solids.

3.4 Projector Augmented Wave Method

A more novel approximation for the orbital part of the wave functions is the projector augmented wave (PAW) method developed by P.E. Blöchl [46]. The general idea is that the space around the atoms is divided into two regions. In the bonding region the wave functions are rather smooth whereas at the region close to the ion cores the wave functions oscillate rapidly. In the PAW method the wave functions are also divided into two parts of which near the core region the wave functions are treated with the partial-wave expansion and with a plane wave expansion outside this spherical region. For materials with rapidly oscillating core wavefunctions the plane wave pseudopotential approximations requires a large basis set. With the PAW methods it is easier to obtain accurate results because of the different kind of treatment of the wave functions in the core region.

We shall briefly look at the main ideas behind the PAW method. The method in full details is presented in the paper by P.E. Blöchl [46]. By adopting the notation used by Blöchl we divide the atomic space into the spherical augmentation region around the ion cores and into the bonding region between the ions. This division is basically similar to the division of space into the core and valence region in the pseudopotential method. We construct a linear transformation from the space of all wave functions orthogonal to the core states to what is called pseudo space (PS). This will be a linear transformation that maps all the physically relevant all-electron (AE) valence wave functions onto computationally practical pseudo wave functions. The particular choice by Blöchl for the transformation is

$$T = 1 + \sum_R \widehat{T}_R, \tag{21}$$

where $\widehat{T}_R$ is a local contribution centered at ion cores and it only acts within the augmentation region Ω_R, R denoting the ions. With this definition the all-electron and pseudo wave functions will coincide outside the augmentation region. The local terms $\widehat{T}_R$ are defined for augmentation regions as

$$|\phi_i\rangle = (1 + \widehat{T}_R)|\tilde{\phi}_i\rangle. \tag{22}$$

Adopting the convention that Blöchl uses we shall call states $|\tilde{\phi}_i\rangle$ PS partial waves and the states $|\phi_i\rangle$ AE partial waves. The AE partial waves can be chosen to be the solutions of the radial Scrödinger equation for isolated atoms.

Within the augmentation region the PS wave functions can be expanded into PS partial waves

$$|\tilde{\Psi}_i\rangle = \sum_i |\tilde{\phi}_i\rangle c_i. \tag{23}$$

Noting that $|\phi_i\rangle = T_R|\tilde{\phi}_i\rangle$ the corresponding AE wave function is

$$|\Psi\rangle = |\tilde{\Psi}_i\rangle - \sum_i |\tilde{\phi}_i\rangle c_i + \sum_i |\phi_i\rangle c_i. \tag{24}$$

Because the transformation T is set to be linear, the expansion coefficients are scalar products $c_i = \langle\tilde{p}_i|\tilde{\Psi}\rangle$ of PS wave functions and some fixed projection function $\langle\tilde{p}_i|$. The projection operator must fulfill the condition $\sum_i |\tilde{\phi}_i\rangle\langle\tilde{p}_i| = 1$ within Ω_R. From this it follows that $\sum_i |\tilde{\phi}_i\rangle\langle\tilde{p}_i|\tilde{\Psi}_i\rangle = |\tilde{\Psi}_i\rangle$ which implies that it must hold $\langle\tilde{p}_i|\tilde{\phi}\rangle = \delta_{ij}$. Altogether this defines a transformation for obtaining the AE wave functions from the PS wavefunctions:

$$|\Psi_i\rangle = |\tilde{\Psi}_i\rangle + \sum_i (|\phi_i\rangle - |\tilde{\phi}_i\rangle)\langle\tilde{p}_i|\tilde{\Psi}\rangle. \tag{25}$$

This way it is possible to choose the PS partial waves such that the remaining degree of freedom can be used to map the physically relevant AE wave functions onto computationally lighter PS wave functions. Accuracy is obtained where it is needed, combined with computational easiness when possible. Fig. 5 illustrates the idea behind the PAW construction.

The core states $|\Psi^c\rangle$ are basically formed in a same manner. With definitions for a PS core wave function $|\tilde{\Psi}^c\rangle$, AE core partial wave $|\phi^c\rangle$ and PS core partial wave $|\tilde{\phi}^c\rangle$, the core states may be expressed as

$$|\Psi^c\rangle = |\tilde{\Psi}^c\rangle + |\phi^c\rangle - |\tilde{\phi}^c\rangle. \tag{26}$$

In contrast to the valence states the projector functions are not needed and the core states are imported from the core states of isolated atoms, similarly to the frozen-core approximation.

3.5 Vienna Ab-Initio Simulation Package

All of the *ab initio* calculations that are part of this thesis have been made with the Vienna Ab-initio Simulation Package (VASP) [47, 48, 49, 50]. The

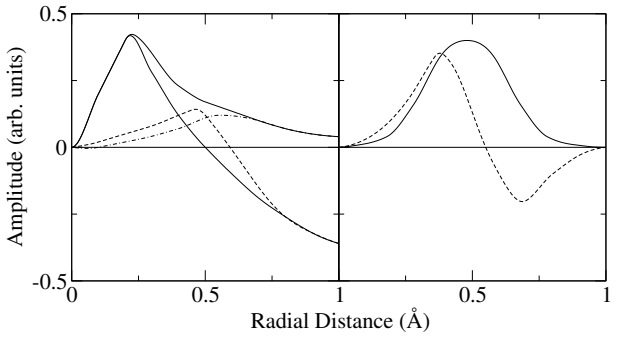

Figure 5: A schematic illustration for PAW potential. On the left hand side AE partial waves $|\phi_i\rangle$ (solid lines) and PS partial waves $|\tilde{\Psi}\rangle$ (dashed and dot-dashed lines). On the right hand side the corresponding projector functions. Illustration is close to the Mn d-channel presentation adopted from [46].

VASP package is an implementation that solves self-consistently with iterative methods the Kohn-Sham equations for the charge density and the Poisson equation for the electrostatic potential from the charge density. We used both ultra soft Vanderbilt type pseudopotentials [45, 51] and the projector augmented waves [46]. The k-point mesh for the Brillouin zone integration for all of the calculations has been generated with the Monkhorst-Pack method [52]. The more specific details on computational parameters and choices have been presented in the corresponding papers as the methods varied according to the needs and the computational resources.

3.6 Local Density of States

As mentioned earlier, the reactivity of the transition metal surfaces is characterized by the density of the electronic states. Especially the local density of states (LDOS) around a specific atom is an interesting quantity when studying the reactivity concepts. The local density of states is defined as

$$\rho(\epsilon) = \frac{\Delta N(\epsilon)}{\Delta \epsilon}, \tag{27}$$

where N refers to the number states as a function of the energy ϵ. In the computational scheme implemented in the VASP the calculation is dis-

cretized

$$N(\epsilon_i) = (\tilde{N}(\epsilon_i) - \tilde{N}(\epsilon_{i-1})), \tag{28}$$

where the total number of states is $\tilde{N}(\epsilon_i) = \int_{-\infty}^{\epsilon_i} \rho(\epsilon) d\epsilon$. The LDOS is computed within a spherical region around the ion cores. The radius of the sphere around atoms can be chosen separately for each atom type in the simulation. There is no unambiguous way to choose this radius. The spheres should, on one hand, cover as much of the space between the atoms as possible but, on the other hand, one would not want the spheres to overlap too strongly. The most common and convenient choice is to use the Wigner-Seitz radius for the atoms [53]. This radius is specific for all of the atom types and we have used in all of the LDOS calculations the Wigner-Seitz radii being supplied in the potential files. The band projected density of states is computed by projecting the electron wave functions onto the spherical harmonics [54]

$$P_{N,l,m,n,k} = \langle Y_{lm}^N | \phi_{nk} \rangle, \tag{29}$$

from which by summing over all the wavefunctions for band one will obtain band projected wavefunctions and densities. This is useful because the bands have different characteristics and they participate in different kinds of bonding phenomena.

3.7 Nudged Elastic Band Method

In the calculation of migration processes one is usually interested in finding the energy barrier which determines the "easiness" of the transition. The path with the lowest transition barrier is called minimum energy path (MEP) and the energetically highest point along this path is called the transition state. The transition state is typically a saddle point of the potential energy surface and it is difficult or impossible to find with a simple relaxation calculation. The nudged elastic band (NEB) method [55, 56] has been developed for finding the minimum energy path and its maximum point between two local minima, and it is implemented in the VASP package.

In the NEB method a chain of subsequent images between two stable configurations is formed. These images are connected to each other with "elastic bands" or springs applying a force to the images. When the chain with the constraint of imaginary spring forces is let to relax, it will finally follow a path where there are forces only parallel to the chain. This path is the

minimum energy path where the physical forces parallel to the chain are compensated with the spring forces. Without this compensation all of the images in the chain would relax to the one of the local minima [55]. The force acting on a chain image i at the coordinate $\vec{r_i}$ is a sum of the physical force and the spring force

$$\vec{F_i} = -\nabla V(\vec{r_i}) + \vec{F_i^s}. \tag{30}$$

Here the spring force with the spring constants k is

$$\vec{F_i^s} = k_{i+1}(\vec{r}_{i+1} - \vec{r_i}) - k_i(\vec{r_i} - \vec{r}_{i-1}). \tag{31}$$

The minimization for the elastic band is done by projecting out the parallel component of the true force and the perpendicular component of the spring force. The force on the image i then becomes

$$\vec{F_i^0} = -\nabla V(\vec{r_i})|_\perp + \vec{F_i^s} \cdot \widehat{\tau}_\parallel \widehat{\tau}_\parallel, \tag{32}$$

where $\widehat{\tau}_\parallel$ is the unit tangent to the path and $-\nabla V(\vec{r_i})|_\perp$ is the component of the physical force perpendicular to the path and is defined as $-\nabla V(\vec{r_i}) - \nabla V(\vec{r_i}) \cdot \widehat{\tau}_\parallel \widehat{\tau}_\parallel$ [55]. The spring forces only affect the relaxation parallel to the MEP, or in other words, the separation of the images along the path. Thus, the choice of the spring forces may be quite arbitrary.

The transition point for a reaction needs to be a saddle point. The NEB method in principle is designed to find the saddle point, but in certain cases it should be verified whether the highest obtained point at the MEP really is a transition state. This is for example possible by moving atoms slightly to see the behavior of a saddle point. However, this is not straightforward in cases of polyatomic molecules as the potential energy surface becomes multidimensional. The other option is to calculate the vibrational spectrum, since at the saddle point the nodes in one direction should be imaginary.

4 Monte Carlo method

The stochastics theory and implementation of the Monte Carlo (MC) methods is discussed in details. Developing a simulation software that implements an MC method for a lattice gas problem has been the greatest single task for this thesis. The program package is based on the one, originally written by J. Heinonen [57], later rewritten by M. Rusanen [58] and which has been rewritten in this thesis to suit for heterogenous systems.

4.1 Introduction

Various numerical methods are nowadays a solid part of every day physics. A great number of problems that we are interested in are too complicated to be solved analytically and for certain problems it can be shown than no simple analytical solution exists. These kind of problems have caused the ongoing development of numerical methods and shown clearly why approximate approaches are needed, developed and widely used [59].

In this chapter we shall focus on the category of numerical methods that are generally called Monte Carlo methods. More specifically we have used methods that belong to Markov chain Monte Carlo (MCMC), which is a class of Monte Carlo methods where the random generation of the system states is based on simulating a suitably constructed Markov chain. For the mathematical background, see for example [60, 61], and for applications in statistical physics, see [62, 63]

Let us begin with a brief introduction to the stochastics and stochastic methods. After this we shall take a look at a physical problem described with the Hamiltonian formalism. The physical problem will be converted into a stochastic model and we shall examine some of the properties the system possess. After this we are going to say a few words about Monte Carlo algorithms for solving numerically the stochastic problem and a few words about the implementation. Altogether this chapter is to be rather general whereas a part of this chapter is reserved for a more specific and detailed description of the lattice gas model and its implementation.

4.2 Stochastics processes and Monte Carlo

4.2.1 Markov Chains

We shall now have a brief glance at the theory of stochastics for examining statistical physics problems. For practical reasons we will deal only with discrete systems and thus discrete phase spaces. To have basic definitions and conventions of stochastics clear we can denote the marginal distribution for a discrete valued random variable in an m-dimensional subspace of the total N dimensional phase space by

$$P(s_m, ..., s_1) = \sum_{s_{m+1} ... s_N} P(s_N, ..., s_{m+1}, s_m, ..., s_1), \tag{33}$$

and the conditional distribution for an m-dimensional subset with fixed values for $s_1, ..., s_m$ we denote as

$$P(s_N, ..., s_{m+1} | s_m, ..., s_1). \tag{34}$$

With these definitions we denote the total joint distribution for all N-dimensions with

$$P = P(s_m, ..., s_1) P(s_N, ..., s_{m+1} | s_m, ..., s_1), \tag{35}$$

which further gives the Bayes' rule [62]

$$P(s_N, ..., s_{m+1} | s_m, ..., s_1) = \frac{P(s_N, ..., s_1)}{P(s_m, ..., s_1)}. \tag{36}$$

Let $s(t) = s_t$ be the state of the system at the time t and may t_n be the time at the n'th step in the series of n successive time steps $t_0 < t_1 < ... < t_n$. If the system is such that the probability for the state s_{t_n} only depends on the immedetiate predecessor

$$P(s_{t_n} = s_{i_n} | s_{t_{n-1}} = s_{i_{n-1}}), \tag{37}$$

the process formed of such steps is called a Markov chain. Of course, one has to be careful when doing this kind of approximation. For a lattice gas model where all the movements are thermal random walk and a waiting time for an event to occur is many decades longer that the transition time itself, the approximation is reasonable. The state here refers to the condition or the configuration of a physical system. For example the state of a Ising model

refers to the configuration of spins in the lattice and in a lattice gas model it refers to the distribution of the particles. The joint probability that the state at time t_n is s_j and at time t_{n-1} is s_i is

$$\Omega_{ij} = P(s_i \to s_j) = P(s_{t_n} = s_j | s_{t_{n-1}} = s_i). \tag{38}$$

For the transition matrix Ω it holds $\Omega_{ij} > 0$ and $\sum_j \Omega_{ij} = 1$. As the weights Ω_{ij} are not time dependent in our case, the Markov chain is stationary. Now, if the probability that the system is in state s_j at the time t_{n-1} is $P(s_{t_{n-1}} = s_j)$, then the probability that the system is in the state s_i at the time t_n will be

$$\begin{aligned} P(s_{t_n} = s_j, s_{t_{n-1}} = s_i) &= P(s_{t_n} = s_j | s_{t_{n-1}} = s_i) P(s_{t_{n-1}} = s_i) \\ &= \Omega_{ij} P(s_{t_{n-1}} = s_i). \end{aligned} \tag{39}$$

From the Markov property it follows that the whole hierarchy is defined by the probability of the initial state $P_0 = P(s_{t_0})$ and the transition matrix elements $\Omega_{ij} = P(s_{t_n} = s_i | s_{t_{n-1}} = s_j)$ giving probability for the states from 0 to $m = n$

$$P(s_{t_0}, s_{t_1}, ..., s_{t_n}) = P(s_{t_0}) \prod_{i=0}^{n-1} P(s_{t_{i+1}} | s_{t_i}). \tag{40}$$

If we look at the first steps of this hierarchy we have

$$P(s_{t_0}, s_{t_1}, s_{t_2}) = P(s_{t_0}) P(s_{t_1} | s_{t_0}) P(s_{t_2} | s_{t_1}). \tag{41}$$

By summing over the spatial configurations s_{t_1} at a fixed time t_1 this will lead to

$$P(s_{t_2}, s_{t_0}) = P(s_{t_0}) \sum_{s_{t_1}} P(s_{t_1} | s_{t_0}) P(s_{t_2} | s_{t_1}), \tag{42}$$

and dividing both sides by $P(s_{t_0})$ gives us

$$P(s_{t_2} | s_{t_0}) = \sum_{s_{t_1}} P(s_{t_1} | s_{t_0}) P(s_{t_2} | s_{t_1}), \tag{43}$$

which is called the *Chapman-Kolmogorov equation* which needs to hold for transition probabilities for a chain to be Markovian [62].

A Markov chain is called stationary if the transition rates are not explicitly time dependent, that is, for all n we have

$$P(s_{t_{n+1}} = s_i | s_{t_n} = s_j) = P(s_{t_n} = s_j | s_{t_{n-1}} = s_k). \tag{44}$$

A stationary Markov chain may be shown to have a series expansion at the small time step limit $dt = t_1 - t_0 \to 0$ of the form [62]

$$P(s_{t_1}|s_{t_0}) = (1 - at)\delta_{(s_{t_1}, s_{t_0})} + dtW(s_{t_1}, s_{t_0}) + O(dt^p), \tag{45}$$

with $W(s_{t_1}, s_{t_0})$ being the transition probability per unit time from s_{t_0} to s_{t_1} and the coefficient $(1 - at)$ being the probability that no transition occur during time t. It follows that $a(s_{t_0}) = \sum_{s_{t_1}} W(s_{t_1}, s_{t_0})$. $O(dt^p)$ is an error term term with $p > 1$. Inserting expression (45) into the Chapman-Kolmogorov equation yields for probability increment within time dt

$$P(s_{t_2}|s_{t_0}) = (1 - a(s_{t_2})dt)P(s_{t_2}|s_{t_0}) + dt \sum_{s_{t_1}} W(s_{t_2}, s_{t_1})P(s_{t_1}|s_{t_0}). \tag{46}$$

First dividing this by dt and then taking a limit $dt \to 0$ further gives

$$\frac{dP(s_{t_2}|s_{t_0})}{dt} = \sum_{s_{t_1}} \big[W(s_{t_2}|s_{t_1})P(s_{t_1}, s_{t_0}) - W(s_{t_1}|s_{t_2})P(s_{t_2}, s_{t_0})\big]. \tag{47}$$

If the system has a discrete set of states then with a new indexing this equation reduces to an expression

$$\frac{dP_j(t)}{dt} = \sum_i (\gamma_{ij}P_j(t) - \gamma_{ji}P_i(t)) \tag{48}$$

which is called the *master equation* [62]. Here $\gamma_{ij} = W(s_{t_j}|s_{t_i})$ is a transition rate from the state s_i to s_j and $P_j(t)$ is the probability that the system is in the state s_j at time t_n.

In the equilibrium the system does not have a real time dependence and clearly $\frac{dP}{dt} = 0$ must hold. The solution

$$\gamma_{ij}P_j(t) = \gamma_{ji}P_i(t), \tag{49}$$

is known as the *detailed balance condition* [62]. Here we denote the transition probability per unit time with W which we further call a transition rate with $\gamma_{ij} = e^{\Omega_{ij}dt}$. From the detailed balance condition we can see that the chain of random function realizations generated have an equilibrium distribution determined by the transition rates given that the chain of states is ergodic, i.e. it can reach every point of the phase space [59].

4.2.2 Monte Carlo method

The physical problem we are solving is the time evolution of a system whose interactions and evolution mechanisms are known and described by a Hamiltonian H. The time evolution of a system initially in the the state $s(t_0)$ at some arbitrary initial time t_0 is described by the equation of motion [64]

$$\frac{ds(t)}{dt} = \frac{-i}{\hbar} H s(t), \tag{50}$$

for which a time independent Hamiltonian has a formal solution

$$s(t) = e^{\frac{-iHt}{\hbar}} s(t_0). \tag{51}$$

Of course we would normally like to find the ground state of the system and to study the time dependent properties in the nonequilibrium case. For a simple Hamiltonian these are usually solvable and the state $s(t)$ may be analytically obtained. But as the Hamiltonian gets more complicated and the system becomes sufficiently large, the time evolution cannot be explicitly solved. When the exact solution is unobtainable, one can apply various approximative and numerical methods to investigate the system.

One of the possible approaches is to give the system stochastic representation and then to use the Monte Carlo integration method to solve numerically the stochastic problem. Let us begin by defining some transition rates γ_{ij} from all possible configurations i to all possible configurations j. The physical model for the system is imported within these probability parameters.

Thus, we define the transition rate matrix Ω

$$\Omega_{ij} = \Gamma_i, \;\; j \neq i \tag{52}$$

$$\Omega_{ii} = -\sum_{j=i} \gamma_{ij}, \tag{53}$$

and the total transition rate $\Gamma_i = \sum_{j \neq i} \gamma_{ij}$ from the state s_i. According to this we define the *transition probability* from s_i to s_j

$$P_{ij} = \frac{\gamma_{ij}}{\Gamma_i}. \tag{54}$$

With these definitions the master equation (48) has an exact solution for the system's state as a function of time t as

$$P(t) = P(0) e^{\Omega t}. \tag{55}$$

It is possible to solve the time evolution of a physical system by generating a time ordered chain of random function realizations. This process samples the phase space of the system randomly obeying the distribution assigned by the transition rates in the master equation. The detailed balance condition assures that the equilibrium state distribution exists and the system will converge towards it if given enough time. In the next subsections we will discuss in details how the transition rates are determined.

4.2.3 Metropolis sampling Monte Carlo method

As mentioned earlier, the Markovian chain of states will converge towards the equilibrium distribution determined by the transition rates. The equilibrium state reached does not depend on how the physical phase space is sampled, once the detailed balance condition is obeyed.

If we were able to determine explicit expression for the partition function of the system then it would be possible to generate an independent sequence of states with the correct rates. However, for a complex system the partition function is not obtainable and that is why the sequence of configurations needs to be formed by some other way. This brings us back to the Markovian chains. A simple fashion to generate the states is to have one initial configuration and in a random manner to evolve the system to another configuration. At this point we do not need to take care of what are these evolution processes. They may be atomic jumps, merging or breaking clusters or anything that takes the system from one point of the phase space to another with a well defined rate.

In the straightforward importance sampling Monte Carlo method the transition rates of these evolution steps do not need to be explicitly known all the time. From a uniform distribution one picks an event and makes an attempt to take this step. The acceptance is randomized against the rate of the process. The step will be taken only if it holds for a uniformly distributed random number $\xi \in (0, 1]$

$$\xi \leq \frac{\gamma_{ij}}{\gamma}. \tag{56}$$

Here we normalize the transition rates, with the total transition rate γ which is the sum of all transition rates. After taking the step or rejecting it the process is repeated.

One can choose the transition rates freely as long as they satisfy the detailed balance condition. As an example we will take a look at the first choice used in statistical physics. It was done by Metropolis *et al.* [65] who chose to use the total energy difference $E_{ij} = E_{s_j} - E_{s_i}$ of the system between the initial and final state of the transition as a parameter with Boltzmann distribution function

$$\gamma_{ij} = e^{-\beta E_{ij}}. \tag{57}$$

The probability of a given state s_i in a classical system is $\frac{e^{-E_{s_i}\beta}}{Z}$, with Z being the partition function of the system [59]. From this it follows that the detailed balance condition (49) for the transition from the state s_i to s_j becomes

$$e^{-\beta E_i}\gamma_{ij} = e^{-\beta E_j}\gamma_{ji}. \tag{58}$$

Thus, it is seen that the energy difference between the states can be used to form the rates.

A chain of states generated this way is time ordered, but the time used is stochastic Monte Carlo time, not physical time. Thus, the Metropolis algorithm does not simulate the dynamics of the system, but it is a method for searching and examining the ground state. If one wants to simulate the dynamical properties of the system, then the algorithm must be implemented by using energetics that take into account the real transition barriers and not only the differences in the total energy.

Similar formulation may be done for transition barriers ΔE_{ij} as well. If we look at Fig. 6 we see that $E_i + \Delta E_{ij} = E_j + \Delta E_{ji}$. Thus, if we choose

$$\gamma_{ij} = e^{-\beta \Delta E_{ij}} \tag{59}$$

$$\gamma_{ji} = e^{-\beta \Delta E_{ji}} \tag{60}$$

for the rates, then it is clear that the detailed balance conditions are satisfied. The importance sampling method has one crucial drawback. If the attempted transition fails, then nothing is done and system prevails its current state. The eminent result of this is a nonzero probability of doing nothing during a program cycle. It becomes obvious that if the event barriers are high compared to the average thermal energy of the system then the time spent on doing nothing becomes significant if not dominant.

In the studies of ensemble averages of an equilibrium system, energetics for sampling the phase space does not need to correspond to any physical dynamics. All that is required is that the processes satisfy the detailed

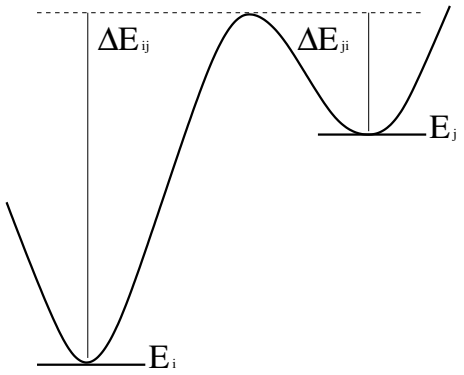

Figure 6: In schematic energy landscape there are shown two local minima with energies E_i and E_j, the transition barrier ΔE_{ij} from the configuration s_i to s_j and ΔE_{ji} from s_j to s_i.

balance condition and that all configurations are reachable. If dynamical properties are studied in equilibrium or the system is not in equilibrium then the processes must be as close to the real physical ones as possible. Otherwise the dynamic physical quantities will not be reproduced correctly. Unfortunately finding the relevant physical processes and their relative barries is difficult and the physical steps are usually very short in the phase space. This means that the relaxation requires more steps since the system changes only very little with each accepted event.

4.2.4 BKL Monte Carlo method

Bortz, Kalos and Lebowitz (BKL) developed a method in which the system is evolved at every simulation cycle to speed up the conducting of the Monte Carlo simulations [66]. The implementation used to obtain the results in this thesis is developed from one by J. Heinonen [57] and rewritten by M. Rusanen [58]. With the current solution it will be straightforward to extend the implementation for kinetic MC. The results in this thesis are obtained with the equilibrium dynamics.

We defined earlier the total transition rate as a sum of all possible transition rates leading away from the current state s_i

$$\Gamma_i = \sum_{j \neq i} \gamma_{ij}. \tag{61}$$

The event is randomly chosen with a uniform distribution based on probability given by

$$P_{ij} = \frac{\gamma_{ij}}{\Gamma_i}. \tag{62}$$

This requires that all of the transition rates are explicitly known throughout the simulation, which makes the implementation of a BKL code trickier than implementing the importance sampling method. In practice, all of the possible configurations and corresponding transition rates are calculated in the initialization of the simulation. Once the rates are calculated they are assigned a label and stored into an array. This way they will be achieved fast without the need to calculate the rates repeatedly every time they are needed during the simulation.

The total transition rate Γ_i defines the decay rate of the state s_i for a system following dynamics

$$\frac{dP_i(t)}{dt} = \sum_{j \neq i} P_j \Omega_{i,j}. \tag{63}$$

The transition probability within the time interval $[t, t + dt]$ from configuration in state s_i to s_j is given by

$$dP_{ij} = \lim_{k \to \infty} (1 - \frac{\Gamma_i}{k})^k = e^{-\Gamma_i t} \gamma_{ij} dt, \tag{64}$$

with t being the time elapsed from the moment when the system was transferred into the state s_i. The probability density distribution then becomes

$$\frac{d}{dt} P_{ij} = e^{-\Gamma_i t} \gamma_{ij}, \tag{65}$$

with two independent random variables, the waiting time t and the configuration in the next state s_j. The time step for the transition is obtained from the waiting time distribution $P(s_i, t) = \Gamma_i e^{-\Gamma_i t}$, by an inverse transform method which yields for the waiting time [57]

$$t = -\frac{ln(\xi)}{\Gamma_i}. \tag{66}$$

This means that physical time is evolved in a stochastic manner by randomizing number $\xi \in (0, 1]$ and calculating the time from the Poisson distribution.

4.3 Observables

During the simulation the simulation time t_i, system configuration $c_i(t_i)$ and corresponding system energy $E_i(c_i)$ are known at each step. From these we are able to calculate certain observables such as island size distribution function, radial distribution function, and so on. Note that here we rather explicitly talk about the different configurations c_i than about the different states s_i. Of course, there is no real difference between them since each of the states s is defined to be one of the possible configurations c.

In general the ensemble average of any observable $\langle A \rangle$ is given by

$$\langle A \rangle = \frac{1}{Z} \sum_c p_{eq}(c(t)) A(c(t)), \tag{67}$$

where $c(t)$ is the configuration of the system as a function of time and $Z = \sum_c p_{eq} e^{-\beta E(c)}$ is the partition function as defined. In the equilibrium the relative probability to find the system in a state c_i within an arbitrary time t_a is given by $p_{eq}(t_a) = e^{-\beta E(c)}$. In the equilibrium the ensemble average can be estimated with the time average of the fluctuating system and it is given by

$$A_e = \frac{1}{t_a} \int_{t_0}^{t_0+t_a} dt A(c(t)), \tag{68}$$

which approaches the ensemble average as $t_a \to \infty$. For discrete systems such as lattice gas models the ensemble average estimate becomes

$$A_e = \frac{\sum_{i=1}^{M} t_i A_i}{\sum_{i=1}^{M} t_i}, \tag{69}$$

where $A_i = A(c(t_i))$ is a realization of the observable A and t_i is the time the system stays in the configuration c_i [57].

4.3.1 Statistical error

According to the central limit theorem the distribution of the average values of random variables with an arbitrary distribution approaches the Gaussian distribution as the number of the measurements increase. This is why the Gaussian distribution is relevant even though in our simulations all of the quantities themselves are Boltzmann distributed.

The unbiased estimator for the mean value of any quantity A with a Gaussian distribution is

$$\langle A \rangle = \frac{1}{n} \sum_{i=i}^{n} A_i, \tag{70}$$

where A_i's are independent realizations of a random variable A. The variance of A is then $\sigma^2 = \langle A^2 \rangle - \langle A \rangle^2$ and the standard error of this estimate is [59]

$$err(A) = \frac{\sigma}{\sqrt{n}}, \tag{71}$$

which is the error caused by finite simulation time, i.e. from a finite set of measures, but also the finite system size causes some statistical error.

Let us do a large number of measurements of an observable A in which case we get a set of values A_i. Then the unbiased estimator for the expectation value of the square of the statistical error is

$$\langle (\delta A)^2 \rangle = \langle [\frac{1}{n} \sum_{i=1}^{n+1} (A_i - \langle A \rangle)]^2 \rangle. \tag{72}$$

Using this and the fact that in the equilibrium state the system must be invariant under time translation (see details e.g. in Ref. [59]) we can define a normalized *time autocorrelation function*

$$\phi_A(t) = \frac{\langle A(t_0)A(t) \rangle - \langle A \rangle^2}{\langle A^2 \rangle - \langle A \rangle^2} \tag{73}$$

where the brackets refer to the average over time. Relaxation time τ_A for a quantity A can then be defined

$$\tau_A = \int_0^\infty \phi_A(t) dt, \tag{74}$$

given that the integral really exists. For many Monte Carlo algorithms this relaxation time tends to diverge near a second order phase transition causing what is called *critical slowing down*. This inefficiency should be kept in mind when dealing with the conditions near second order phase transitions.

4.3.2 Radial distribution function

The radial distribution function tells us on average how many neighboring atoms, the same or different kind, an atom tends to have at different distances. It is calculated by going through all the lattice sites and calculating the number of atoms of each kind at different distances within a certain limit.

The radial distribution function is used to monitor the changes in the structures formed in the system. The possible ordering of the system on different length scales is seen on the radial distribution function. As well it reflects the formation of a certain type of pairs and island shapes and sizes.

4.3.3 Island-size distribution function

The island-size distribution function is observed applying the Hoshen-Kopelman [67] algorithm for calculating the sizes. The distribution may be observed after every MC step. The island size is determined separately for different atom types and also for empty areas. The nearest sites belong to a same island if they are occupied by an atom of a same type or they are both empty sites.

4.4 General implementation of BKL-method

In the BKL Monte Carlo it is necessary to know all the transition rates connecting different states to each other. This makes the method more difficult to be implemented, but on the other hand it makes the code significantly faster. This is most easily done by calculating the transition rates in the beginning of each simulation and updating those that change during the evolution. And of course, most of the transition probabilities will be trivially zero since all the states cannot be reached within a single step from any given initial state.

The basic structure of a lattice gas BKL Monte Carlo code is:

1. Find the next transition $c_i \rightarrow c_j$ using relative transition rates γ_{ij}.

   Finding the transition may be done in several ways as long as the method picks the transition with a correct probability. The search

procedure may be arranged as a binary tree, a list or similar. The binary tree structure will be discussed in details later.

2. Execute the transition. Update lattice, configuration numbers and transition rates. A transition means that the spatial configuration of the system is chanced, which means that the set of possible events and their probabilities are altered as well. All those transitions rates that have changed must be refined before choosing the next event.

3. Update the search structure for finding the site. When the transition rates have changed, also the search structure need to be updated.

4. Update physical time and any other needed variables. After the configuration has been changed, one needs to take care that the time is evolved correctly.

5. Calculate desired observables and check whether the criteria for stopping the simulation was reached. If not, then start a new cycle from step one.

4.5 Implementation of the lattice gas BKL Monte Carlo method

So far the description of the Monte Carlo method and related algorithms have been as general as possible. The system we are dealing with is a diatomic lattice gas and the following concerns more specific implementation of the BKL Monte Carlo. In a lattice gas model we assume a regular 2D lattice, for example in this case, an ideal atomic surface of the (100) direction.

On this lattice we have sites which may be empty or occupied by an adatom. The system is evolved by letting the atoms to jump from one site to another. Our model is based on jumps from a site to its immediate neighbor site. The transition rates are determined for the monoatomic migrations from site to site or by the total energy difference between the initial and final configurations. The transition probability depends on the Boltzmann factor of the corresponding energy difference. Thus, the jumps have relative probabilities that have exponential ratios. How the event is actually chosen will be discussed later on.

The radial distribution function calculated by going through the lattice once for all occupied lattice sites tells us how many atoms of each type is at different distances. The radial distribution function is normalized with the number of lattice sites at different distances. This way it gives the relative occupancy of different types at all distances within a certain radius. The island size distribution function is measured separately for all different atom types as well as for the empty areas.

In general case the BKL may be implemented as kinetic Monte Carlo method which obeys the real dynamics of the systems with energetics based also on the diffusion barriers and not on the total energy differences alone. However, in our calculations we have used an implementation based on the total energy differences for the transitions neglecting the real diffusion barriers. The results in this thesis have been calculated with no deposition and thus the particle number is preserved. However, the current implementation already includes the option to include the real dynamics as well as the gas phase into the system.

4.5.1 Diffusion energetics and transition rates

The jump probability and choice of the jump event are based on the transition rates which are essentially functions of the total energy difference ΔE between the initial and final state of the transition.

The relative probability for the jump is

$$\gamma_{ij} = \begin{cases} Ce^{\frac{-\Delta E}{k_b T}}, & \text{if } \Delta E > 0 \\ C, & \text{if } \Delta E \leqq 0 \end{cases}$$

with a constant prefactor C. The prefactor may be derived from the diffusion experiments, but in this case it is used to scale the transition rates to a convenient range. From the transition rates the process to be executed is randomized. The transition rates are exponential functions of the corresponding energy term, and thus from the transition rates the transition is chosen according to a uniform distribution.

How these barriers are determined is a problem of its own. One of the widely used possibilities for atomic systems is to apply some other numerical simulations, e.g. electronic structure calculations, molecular dynamics and such methods to determine the needed energetics (see for an example a book by Axel Groß [28]).

The effect of the neighborhood can only be considered to a certain extent because the complexity increases when the interaction area size increases. On the other hand, it is essential to include all the relevant processes into the model if one is interested in the dynamical properties of the system. For our implementation, the energetics are calculated for monoatomic jumps with an *ab initio* method, taking nearest and next nearest neighbor interactions into account. The neighborhood that is considered when calculating barriers or total energy differences is called the interaction area.

With the coupling terms J the Hamiltonian will be

$$\widehat{H} = \frac{1}{2} \sum_{<i,j_{nn}>} J^{nn}_{\sigma_i \sigma_j} + \frac{1}{2} \sum_{<i,j_{nnn}>} J^{nnn}_{\sigma_i \sigma_j}, \tag{75}$$

where the first sum goes over nearest neighbors (nn) and the second sum over next nearest neighbors (nnn) with J_{σ_i,σ_j} giving the corresponding bond energy. The bond between atoms in the model refers to the interaction energy of neighboring atoms and the interaction can be either repulsive or attractive. The energy difference ΔE will be the difference in the total energy between the initial and final state of the transition. In other words we have a bond counting model which takes into account the number and type of the nearest and next nearest adatoms. The coupling constant values that were used are seen in Table 1. These values have been obtained by fitting a model with six parameters into a large set of data. The original energetics data has been taken from Paper **IV**.

Bond type	Bond Energy (eV)
J^{nn}_{OO}	0.37
J^{nnn}_{OO}	0.12
J^{nn}_{CuO}	0.30
J^{nnn}_{CuO}	0.04
J^{nn}_{CuCu}	−0.34
J^{nnn}_{CuCu}	−0.09

Table 1: Energetic values for different types of interactions i.e. bonds. Indeces nn refer to the nearest neighbors and nnn to the next nearest neighbor. The negative sign tells that the interaction is attractive (only between two Cu atoms) and a positive sign refers to a repulsive interaction.

The parameterization of the MC energetics has been made by a method of least squares from a large set of processes (Paper **IV**). Because of the fitting,

the parameters are not too sensitive for a single diffusion barrier calculations. Different approximations in the DFT scheme can give slightly different barries for the diffusion processes. However, these differences should be negligible. The essential condition for the accuracy is that the relative ordering of qualitatively different processes has to be the same. Moreover, we have not explicitly checked how sensitive the results are to the choice of the parameterization.

4.5.2 Choosing events

The principle of choosing events was introduced earlier. The actual implementation may be done in several ways of which we have chosen to use the one relying on a binary tree structure [68]. The number of bottom level nodes in the tree is chosen to exceed the number of lattice sites and then by starting from "the left hand site" we place the total rates for every site of the lattice into these nodes (see Fig. 7).

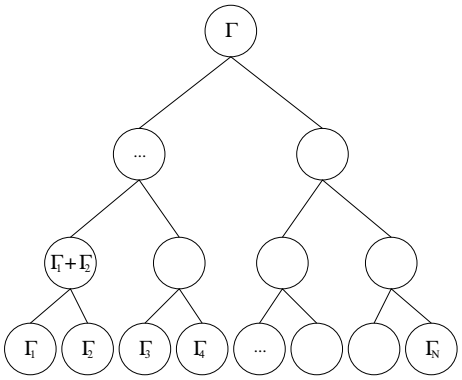

Figure 7: A binary tree for choosing the event. The bottom level nodes are filled with the transition rates of the lattice sites and every parent contains the sum of its children's values.

Here we denote with Γ_i the transition rate summed up from transition rates for all four jump directions. When all sites have a corresponding node at the bottom level then the tree is summed up such that each node gets a value which is the sum of its two children. What becomes to the top node is called the total transition rate Γ.

Now we essentially randomize a number $r \in (0, \Gamma]$ from a uniform distribution. If the rate of top node's left child is $\Gamma_{left} > r$, then we proceed to the

left child and do the same comparison to its children. In the opposite case we choose the right child and re-scale the random number $r_{new} = r - \Gamma_{left}$. This process is done over and over again until the bottom row is reached which means that the site is chosen. The same procedure is extended to choose the jump direction after the site has been found.

From a computational point of view the choice and implementation of the search structure and the updating scheme are essential. Almost all of the computational time is spent on doing these two things. A binary tree as a search procedure is good because the increment of the search time grows as a logarithm of the size of the simulation lattice. The updating of the configurations has binary operations in its core implementation for a reason that it is significantly faster than other options we have come up with.

5 Results

This section is divided into two parts. In the first part the reactivity of PdAg alloy surfaces and the catalyzed CO oxidation are discussed. In the latter half, the oxidation and oxygen induced reconstruction of Cu(100) are considered.

We consider the adsorption of O atoms and O_2, CO and CO_2 molecules on different surfaces. To be able to calculate the adsorbtion energies we need the vacuum energies for the adsorbates. The adsorption energy E_{ads} is defined as

$$E_{ads} = E_{system} - E_{slab} - E_{adsorbate}, \tag{76}$$

where E_{system} is the total energy of the system with adsorbate on the surface, E_{slab} is the total energy of the clean slab and $E_{adsorbate}$ is the energy of an isolated adsorbate atom or molecule.

5.1 PdAg surfaces and catalyzed CO oxidation

Due to the strong surface segregation, the PdAg alloy that has two thirds of palladium in total, has only 5% Pd concentration on the (111) and even less on the (100) surface [5]. This has led us to choose a surface slab model with a 3×3 surface cell and three layers for the (111) surface. The slab is formed of Ag atoms of which one in the surface layer is replaced with a Pd atom giving the Pd concentration of 11%. Pd, Ag and PdAg alloy have a face centered cubic (fcc) bulk structure. The reactivity of the PdAg alloy surfaces and the oxidation of CO are considered in details in Papers **I-III**.

The experimental studies by Wouda *et al.* [69] have shown that the concentration of Pd atoms at the (111) surface is very low. Even lower is the number of Pd clusters of two or three atoms, that are suggested to be the active dissociation sites [5]. Thus, the chosen model, with only one or two Pd atoms in the slab is close to what the PdAg surface is in the real conditions, keeping in mind that the bulk beneath this kind of a surface consist mainly of Pd atoms. The experiments by Wouda *et al.* studied flat surfaces with no steps. We have also concentrated on the step-less surfaces. However, the effect of steps is an interesting subject, which should be studied in the upcoming projects.

5.1.1 Reactivity of PdAg surfaces

The adsorption energetics on transition metal surfaces is related to the interaction between the p-band of the adsorbates and the d-band of the surface atoms. This hybridization is also a key to the catalysis. If the adsorbates have their atomic or molecular orbitals, i.e. the electronic states, on very different energies, then it is unlikely that the hybridization will occur. In the transition metal catalysts, the width of the d-band is typically the order of several eV's. Thus, it is quite propable that the narrow p-bands of adsorbates overlap with the d-band of the metal surface. Once the adsorbate's orbitals have strong hybridization with the orbitals of the surface atoms, then a channel for a charge transfer from one adsorbate to another may occur. When the charge transfer is possible the adsorbates can form a mutual bond.

The reactivity of surfaces can be described in the terms of LDOS [70]. The Pd and Ag have different kind of d-bands in the bulk, but more than that Pd possesses a really strong surface state. The LDOS of a Pd atom in the bulk and a Pd atom at the surface are strongly different, as can be seen in Fig. 8 (a). The LDOS for Ag is quite the same for a bulk atom and for a surface atom, see Fig. 8 (b). Also, the whole d-band of the Pd atom is on higher energies than the d-band of the Ag atom which reflects a different kind reactivity. Especially the LDOS of the Ag atom at the Fermi-level is zero both in the bulk and in the surface but for the surface Pd atom the density of states at the Fermi-level is nonzero.

5.1.2 Dissociation of O_2 on PdAg(111)

Since the Pd atom on the PdAg(111) surface seems to be the reactive site, the dissociation of O_2 on the Pd sites has been studied [71]. The dissociation barrier was calculated for Ag(111) surface with no Pd and for PdAg(111) with one Pd atom and with two Pd atoms [71] in the 3×3 surface cell. The calculated configurations are seen in Fig. 9 and the obtained minimum energy paths in Fig. 10.

The extracted dissociation barriers together with the adsorption energies for the dissociated molecules are seen in Table 2. As the Pd concentration increases the O_2 binding to the surface decreases and even more so does the dissociation barrier. This significant decrease gives a reason to assume

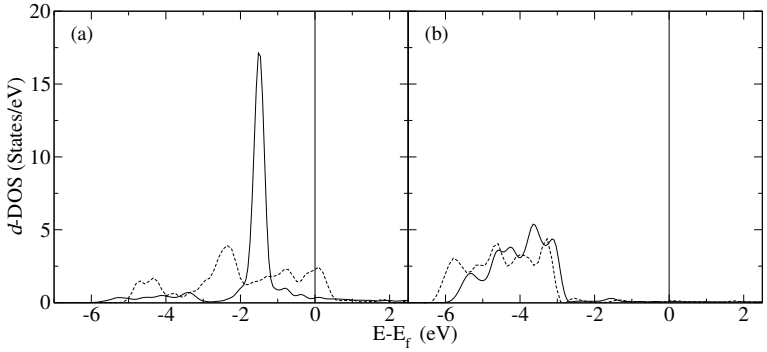

Figure 8: (a) The LDOS of the *d*-band of Pd atom in the bulk Pd (dashed line) and a Pd atom in the PdAg(111) surface (solid line). (b) The LDOS of the *d*-band of an Ag atom in the bulk Ag (dashed line) and an Ag atom in the PdAg(111) surface (solid line). The on-surface Pd and Ag atoms are nearest neighbors to each other.

that the reaction rate for dissociation in the real conditions near small Pd clusters on the Ag(111) surface is enhanced. When considering the oxidation of CO, alloying some Pd into Ag might speed up the catalysis. Pd enhances on one hand the CO adsorption and on the other hand the dissociation of O_2 molecules to provide the needed O atoms. As already mentioned, it is difficult to say which of the process steps is the rate limiting step.

Table 2: Adsorption energies E_{ads} for an dissocated O_2 molecule and dissociation barriers E_{dis} for an O_2 molecule on Ag(111) and PdAg(111) surfaces. Energies are compared to the energy of a O_2 molecule in the vacuum [71]. Results that are not currently available are marked with NA.

	E_{ads} (eV)	E_{dis} (eV)
Ag	−1.13	1.26
Pd_1Ag	−1.12	0.76
Pd_2Ag (a)	−0.98	NA
Pd_2Ag (b)	−0.74	0.18

Our results for the effect of Pd atoms in the dissociation of O_2 are in agreement with experimental results. Wouda *et al.* [69] have shown that oxygen atoms on the PdAg(111) surface are selectively adsorbed on the Pd sites. The Pd atoms are mostly isolated by Ag atoms and the experimental sticking coefficient has also been seen to be extremely small as on pure Ag(111)

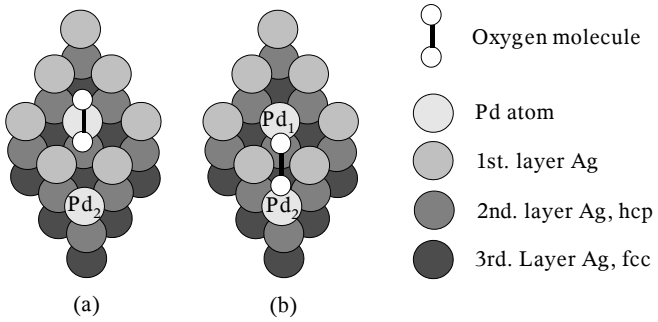

Figure 9: Considered dissociation geometries of O_2 molecule on Ag and PdAg surfaces. The geometry (a) is considered for Ag, Pd_1Ag, and Pd_2Ag surfaces and the geometry (b) for a Pd_2Ag surface only.

surfaces [72]. This experimental observation suggests that an ensemble of neighboring Pd atoms is needed to dissociate O_2 molecules. The low overall sticking seen in the experiments verifies that the clusters of Pd atoms in the surface are rare as also seen in the STM experiments [69]. Probably these Pd sites can also be poisoned rapidly by adsorbed O that would further explain the low experimental sticking coefficients. This is supported by our observation that the adsorption sites next to Pd atoms are the most stable ones for O.

5.1.3 O and CO adsorption on PdAg surfaces

On the (111) directed surface there are three different high symmetry sites, one at the top site above the surface atoms and two different hollow sites. An hcp hollow site is a site above the atom in the second layer and an fcc site is above the atom at the third layer.

The adsorption of O on clean surfaces and the adsorption of CO on oxygen pre-covered surfaces were studied. Ag, Pd and PdAg surfaces are all equally capable of binding O atoms. The O pre-covered Ag(111) does not bind CO, whereas Pd(111) and PdAg(111) surfaces do, see Table 3 and Paper **I**.

In every case the hollow sites are preferential adsorption sites. On the alloy surface the fcc-hollow site next to the Pd atom is the most stable adsorption

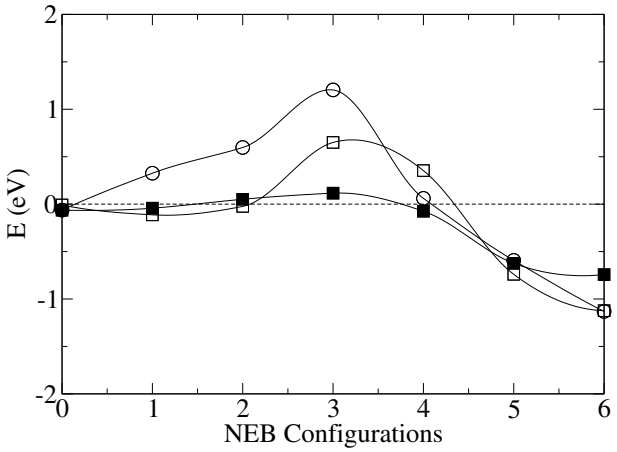

Figure 10: NEB graphs for the dissociation of O_2 on Ag(111) (open circles), $Pd_1Ag(111)$ (open squares) and Pd_2Ag geometry (b) (filled squares). In the initial position (0) O_2 molecule is 2.8 Å above the surface and in the final configuration (6) two oxygen atoms are adsorbed onto the surface. The zero level corresponds on the energy of a system with a O_2 molecule far away from the surface [71].

Table 3: Adsorption energies E_{ads} for O on clean and for CO on O pre-covered Ag(111), Pd(111) and PdAg(111) surfaces. The O atom is adsorbed on the fcc hollow site and in the case of PdAg surface on the hollow site next to the Pd atom which is the most stable adsorption site. The CO molecule is adsorbed on the hollow site next to the same surface atom that O is adsorbed, see Fig. 11 (a) and (b).

	O	E_{ads} (eV)	CO	E_{ads} (eV)
Ag	fcc	-3.8	fcc	-0.1
Pd [73]	fcc	NA	fcc	-1.9
PdAg	fcc	-3.7	hcp	-0.9
PdAg	fcc	-3.7	fcc	-0.6

site for O. The Pd seems not to have any great effect on the O adsorption. The adsorption energies at the hollow sites are all between -3.5 eV and -3.7 eV. The hybridization between the Pd $4d$-states and O $2p$-states is quite different on the hollow and on the top sites. At the top site the O states are shifted towards to the higher energies, which relates to the weaker bonding. There is no hybridization between the surface and O s-peak, which

is roughly at 1 eV higher in the energy at the top site than at the hollow site next to Pd atom, see Paper **I**. On the O pre-covered surface, the CO is also adsorbed at the hollow site. The adsorption energy on different hollow sites differ from −0.34 eV to −0.87 eV. The differences tend to be greater than those for the O adsorption.

5.1.4 Oxidation of CO on PdAg(111) surfaces

The oxidation of CO on the catalytic surfaces follows the Langmuir-Hinshelwood process. The CO molecule and O atom are both adsorbed on the surface where they diffuse to meet each other and they react forming a CO_2 molecule which then desorbes from the surface. Both the O atom and the CO molecule are adsorbed on the fcc hollow sites, CO vertically carbon head closer to the surface. The considered initial configurations are seen in Fig. 11 (b). In the final configuration of an NEB calculation the CO_2 molecule resides vertically above the surface.

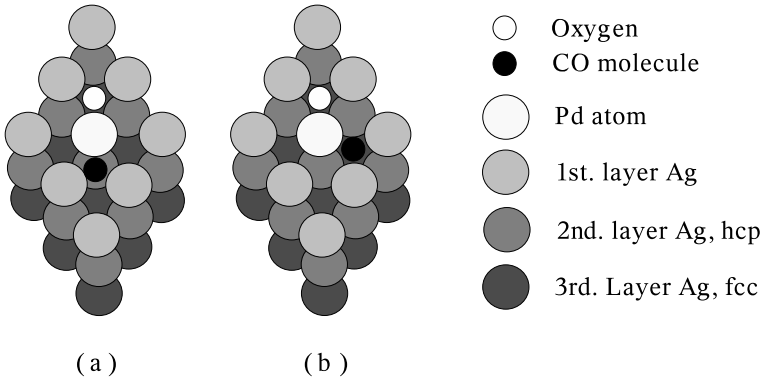

Figure 11: (a) The most stable adsorption geometry on PdAg surface. (b) The initial configuration for considered NEB calculations, where the CO molecule and O atom are adsorbed on the nearest fcc hollow sites.

The effect of alloying is seen on the reaction barriers for the oxidation and on the adsorption energies. The reaction barrier should be small and at least less than the desorption barrier for the reaction combounds. Fig. 12 shows the minimum energy paths for CO and O to form CO_2 on the Pd(111) [73], Ag(111) and PdAg(111) surfaces (Paper **II**). The alloy surface is the most suitable for the CO oxidation having a smallest barrier for the reaction. On the Ag(111) surface the problem is that the clean surface is not capable to bind CO molecules.

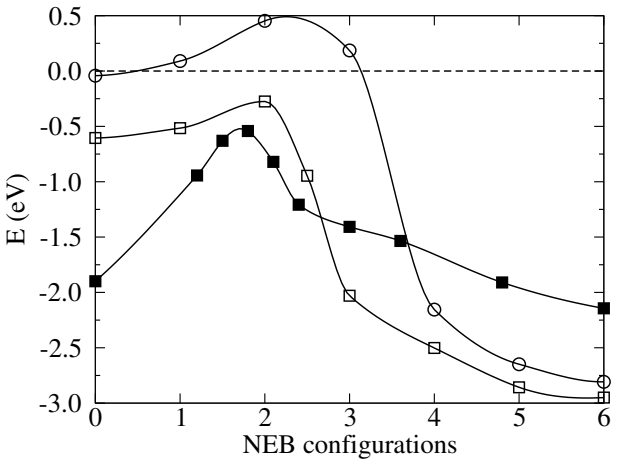

Figure 12: Energetics calculated using the NEB method for the CO oxidation reaction on Pd(111) (filled squares) [73], on Ag(111) (open circles) and on PdAg(111) (open squares) between the initial (0) and final (6) state. In the initial state O and CO are at the nearest-neighbor fcc sites (see Fig. 11), in the final state CO_2 is lying horizontally above the surface. The zero of the energy corresponds to CO desorption energy from the O pre-covered surface in each case. For more details see Paper **II**.

Our purpose has been to study the effect of alloying on electronic structure and the hybridization. We concentrate in Fig. 12 on the processes on the surface. For this reason the zero energy level is taken to be the desorption level of the CO molecule. This way it is easy to see whether the reaction could happen or not, regardless of what the energy for the O_2 molecule in vacuum. We have not separately verified that the maximum energy point along the minimum energy path given by the NEB calculations is the transition state. We are confident that, with geometries that are this simple, the NEB is capable to find the correct transition state.

It is shown that the Ag(111) surface cannot effieciently catalyze CO oxidation. The Ag(111) surface lacks the capability of dissociating the O_2 molecules and it binds the CO molecules too weakly to be effective. Both of these incapabilities can be promoted with introducing Pd atoms on the Ag(111) surface as the Pd sites bind more strongly the CO molecules. Experimental studies have shown small clusters of Pd atoms to be the reactive sites for O_2 dissociation [69]. This is profitable since pure Pd surfaces binds O atoms perhaps too strongly to work efficiently at lower temperatures, not to mention that silver is a whole lot more common and more inexpensive

material than palladium.

The principle that the interaction between reaction compounds and the catalytic surface should not be too weak nor too strong, is known as a Sabatier's principle [1]. More precisely, the Sabatier's principle identifies the universal relation between the activation energies and heats of adsorption for particular classes of reactions.

5.2 Oxidation of Cu(100) surface

The oxidation of a Cu(100) surface and the oxygen induced reconstruction are studied with *ab initio* methods and with stochastic Monte Carlo simulations. The dissociation of O_2 molecules, adsorption of the O atoms and O_2 molecules and diffusion of O and Cu adatoms on the clean and reconstructed Cu(100) surfaces are discussed. Also, the island formation and self-assembling of CuO structures on the Cu(100) are considered. The dissociation of the O_2 molecules and adsorption of the O atoms and O_2 molecules on the Cu(100) surface have been discussed in Paper **IV** and on the reconstructed Cu(100) in Paper **V**. The island growth and the self-assembling of the oxide structures have been studied in Paper **VI** together with further discussions on the O induced reconstruction of the Cu(100) surface.

5.2.1 Oxygen dissociation on Cu(100)

The experimental sticking coefficient of the O_2 molecules on the Cu(100) surface is low at small incidental energies. This is caused by a small dissociation barrier [8]. In the potential energy surface (PES) calculations this barrier is not seen. PES studies by Puisto and Alatalo in Paper **IV** show direct dissociation without a barrier on the top and at the bridge sites and a molecular adsorption at the hollow site. This discrepancy between the experiments and computational studies can be attributed to the steering effect. The steering effect is taken into account in the molecular dynamics studies, where the incident molecule may drift to an energetically favorable trajectory with a suitable orientation. The further molecular dynamics studies also confirm the existence of a small dissociation barrier on the clean Cu(100) [74].

5.2.2 Oxygen adsorption and diffusion on Cu(100)

The adsorption of O was studied on different co-adsorption geometries together with Cu adatoms on the Cu(100) surface. The adsorption energies for the O atom and O_2 molecule are seen in Table 4. Of course, in normal conditions oxygen exists as molecules in the gaseous phase. The comparison here addresses the high strength of the O-surface binding and the O-O repulsion relative to it. For two and three neighboring O atoms, the adsorption energy per atom is slightly decreased because of the O-O repulsion. The adsorption calculations correspond to O coverages from $\frac{1}{16}$ ML to $\frac{3}{16}$ ML of oxygen. Typically the experimental results such as experiments by Fijita *et al.* [75] are performed at higher O coverages up to $\frac{1}{3}$ ML of O, after which the reconstruction begins to form.

The oxygen adsorption on sub-surface is energetically not-favorable at low on-surface oxygen coverages on Cu(100). The increasing on-surface oxygen coverage seems to stabilize the sub-surface adsorption [76]. Similar behavior has been seen on Cu(111) where sub-surface adsorption is energetically unfavorable [77]. On Cu(111) the oxygen forms bulk Cu_2O cuprous oxide structures on the surface, which is the stable phase under catalytic working conditions [77]. Even though the structure of Cu_2O is different, the situation is quite similar to the reconstructed Cu(100) oxide surface.

The adsorption of the O_2 molecule is weaker which is understandable since the O_2 molecule is more inert compared to the radical O atom. The diffusion barrier for the O_2 molecule is 1.1 eV from a hollow site to another hollow site. The O_2 molecule is adsorbed on a horizontal position at the hollow and bridge sites. In the diffusion process, the O_2 molecule migrates in an almost horizontal position. The minimum energy path obtained with an NEB calculation is seen in Fig. 13. For a more detailed analysis see Paper **IV**.

According to the *ab initio* calculations the barrier for Cu atoms to diffuse on the Cu(100) surface is lower than the diffusion barrier for the O atoms. This leads to an assumption that Cu might be the more mobile species on Cu(100), but that cannot be said surely based on the barrier alone. The migration barriers for Cu atoms vary from 0.25 eV to 0.84 eV and for O from 0.45 eV to 0.94 eV. The self-diffusion barrier for Cu is lowered by the presence of O adatoms whereas the effect of Cu on O diffusion is less pronounced. In addition to the migration barriers, it was found that there

Table 4: Adsorption energies E_{ads} per atom for the O atom and for the O_2 molecule on the Cu(100) surface. Energies for O atoms residing in the hollow sites and for O_2 molecule in the hollow and bridge site. The adsorption energies of the O atom (O_2 molecule) is compared to the energy of the atom (molecule) in the vacuum.

	Config.	E_{ads} (eV)
1O	○	−5.44
2O	○○	−5.21
3O	○ ○○	−5.14
O_2	hollow	−1.91
O_2	bridge	−0.82

is an attraction between Cu adatoms and repulsion between O adatoms and between O and Cu adatoms (Paper **IV**).

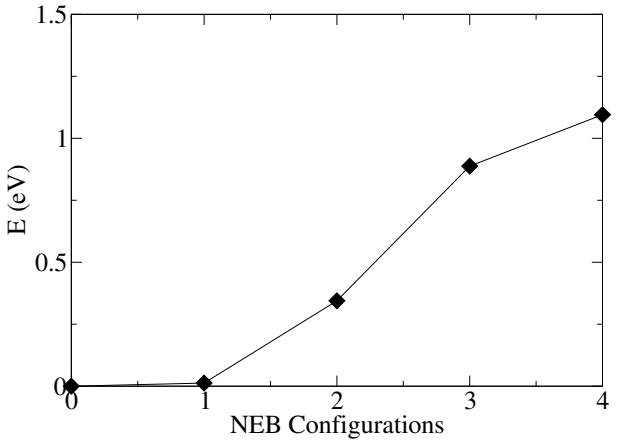

Figure 13: O_2 diffusion on the Cu(100) surface. The NEB configuration 0 corresponds to the geometry where the O_2 resides at the hollow site and the configuration 4 corresponds to O_2 at the bridge site. At the both sites, O_2 is adsorbed in a horizontal position.

5.2.3 Oxygen dissociation on reconstructed Cu(100)

One of the interesting features of the Cu(100) surface is the oxygen induced reconstruction. As the oxygen coverage on the surface increases it forces the

surface to form Cu(100)-$(2\sqrt{2} \times \sqrt{2})R45°$-O missing row reconstruction, see a schematic representation in Fig. 14. The missing row reconstruction is seen to begin to form at the coverages of 0.34 ML of oxygen and it is complete when the O coverage reaches 0.50 ML [10, 17].

It seems that the reconstruction is solely coverage driven in the sense that temperature and pressure do not affect the formation of the reconstruction. According to Stolbov *et al.* the driving force behind the reconstruction is the long range Coulomb repulsion of surface O atoms [10]. Merrick *et al.*, on the other hand, state that according to their computational studies the long range interactions should play a lesser role.

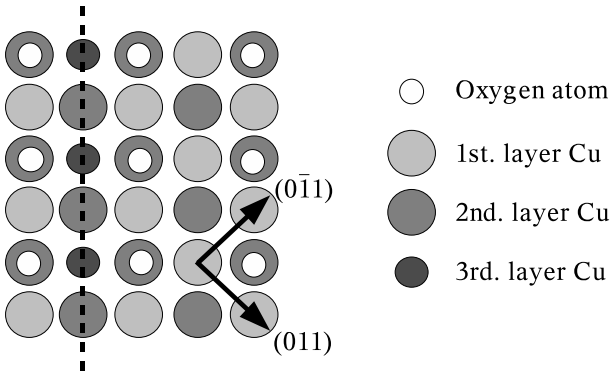

Figure 14: A schematic representation of the missing row Cu(100)-$(2\sqrt{2} \times \sqrt{2})R45°$-O surface. The missing row on the surface layer is denoted with a dashed line.

The reconstructed surface is stable and more inert to the O_2 adsorption and dissociation than the unreconstructed Cu(100). Experimental observations on the sticking coefficient as well as computational molecular dynamics and total energy adsorption studies reveal that the adsorption and dissociation of oxygen on the reconstructed surface are weaker than those on the unreconstructed Cu(100) [8, 74] and Paper **V**. The experimental molecular-beam surface-scattering experiments show only a weak increase of the sticking coefficient with respect to the increasing kinetic energy of the incident molecules. This suggests that on the reconstructed surface the adsorption of O_2 is mediated either by a precursor state or a steering mechanism. The calculated dissociation barriers are high being between 3.2 eV and 4.6 eV. The dissociation and adsorption of O_2 and the adsorption and diffusion of Cu and O adatoms on the reconstructed surface are considered in details in Paper **V**.

5.2.4 Oxygen adsorption and diffusion on reconstructed Cu(100)

The adsorption energies of O_2 molecules on the reconstructed Cu surface are between -0.1 eV and $+0.8$ eV. The low or even positive adsorption energies together with the high dissociaton barrier tells about a strong repulsion between the surface and O_2 molecules. The weak binding observed hints that the O_2 molecules would easily diffuse away from the reconstructed parts of the surface towards the areas with more excess Cu. The passivity of the reconstructed surface is explained by the missing of free Cu bonds as they are already saturated with the surface oxygen. On the reconstructed islands copper and oxygen form oxidule (Cu_2O) [10].

The diffusion of O and Cu adatoms on the reconstructed parts of the surface is slow both along the direction of the missing row and also perpendicular to it. The diffusion barrier for the O adatom along the missing row is roughly 1.4 eV and for the Cu adatom almost 2 eV, whereas the migration barriers for O and Cu adatoms on the unreconstructed Cu(100) surface are less than 1 eV. This gives a reason to believe that the reconstruction island formation is dominated by the dissociation and diffusion processes on the unreconstructed parts of the surface rather than on the reconstruction islands, see Papers **IV** and **V**.

5.2.5 Cu and O structures on Cu(100)

The O and Cu structures on Cu(100) were studied with statistical Monte Carlo simulations. We have used several different O and Cu adatom coverages and few different temperatures to examine the island and Cu-O structure formation. We were able to reproduce the c(2×2)-O domains seen in the experiments [75], verifying the interpretations of the experimental measurements (Paper **VI**). The experiments by Fujita *et al.* [75] were made in in 450 K surface temperature and the temperatures used in our MC simulations were 300 K, 450 K and 600 K.

When the coverage of Cu and O adatoms increases we see the formation of larger Cu islands and c(2×2)-O domains in between them. The c(2×2)-O domains are separated by mobile domain boundaries. The mobility of the domain boundaries is a result of the mobility of the O adatoms. According to the MC simulations, oxygen is more mobile species on the Cu(100) even if the *ab initio* diffusion barriers for O are higher than those for Cu. The low

mobility of Cu is caused by the stability of Cu islands where only on-edge diffusion appears.

Because of the strong repulsion the oxygen will not have nearest neighbor O or Cu atoms as long as there is room for O to form c(2×2)-O domains. After the coverage increases the formation of Cu-O nearest neighbor pairs occurs. This will initiate the formation of the reconstruction on the Cu(100) surface. On higher O coverages the reconstruction geometry minimizes the strong O-O and O-Cu repulsion present on Cu(100). In our simulations these domains are clearly visible, as seen in Fig. 15.

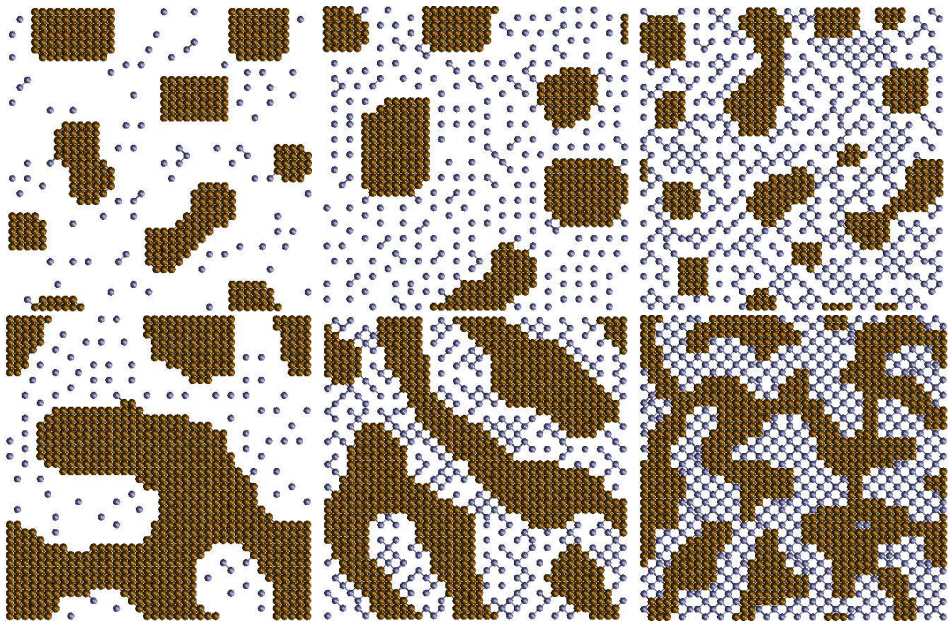

Figure 15: Snapshots of the simulation lattice in equilibrium. Darker and denser dots represent Cu (ochre in colors) and lighter and more dilute O (blue in colors) at $T = 600$ K. On the left hand side 0.05 ML O, in the middle 0.15 ML O and on the right hand side 0.25 ML O. On the first row 0.25 ML Cu and on the second row 0.50 ML Cu. Nearest neighbor adatoms touch each other and the next-nearest neighbor adatoms are linked with a stick. The vertical and horizontal directions are $[0\bar{1}1]$ and [011], respectively.

A locally ordered pattern was observed in the scanning tunneling microscopy (STM) experiments [75]. The c(2×2) pattern seen in the low energy electron diffraction (LEED) experiments by H. C. Zeng *et al.* [78] corresponds to the four-spot structure. The width of the observed diffraction spots in

the LEED pattern was attributed to the strong distortion of the c(2×2)-O structure and to the lack of the long range ordering of adatom oxygen. Our simulation results are in good agreement with the experimental observations. Based on the experiments it has been suggested that the c(2×2)-O structure with small domains would be a consequence of O-O interaction that would generally be repulsive, but on certain short distances attractive [75, 79]. Our simulations are based solely on the local O-O repulsion and we are able to reproduce the c(2×2)-O implying that it is actually caused by repulsive forces between O adatoms together with repulsive O-Cu interaction.

The formation of nearest neighbor O-O pairs only occurs at high coverages because of high O-O repulsion. Similarly there will be nearest neighbor O-Cu pairs only when the overall coverage, especially the coverage of O reaches a certain level where there is no room for O to form distinct c(2×2) domains.

In general, the processes on the Cu(100) surface are dominated by the O-O repulsion. The repulsion is quite strong, but we have not tested the sensitivity of the system to the strength of the interactions. The local c(2×2)-O structure as well as the absence of the long range ordering is due to this repulsion. Also this repulsion is the driving force behind the reconstruction, since in $(2\sqrt{2} \times \sqrt{2})R45°$-O there are no direct O-O nearest neighbors and the Cu-O structures are forming Cu_2O compounds with covalent bonding via hybridization of the O p-band and the Cu d-band [10, 80], which is energetically favorable.

6 Conclusions

Catalytic efficiency of a transition metal surface depends on a few principles. Especially considering the oxidation, the surface must be capable of dissociating O_2 molecules. The second goal is that the surface must adsorb reactants, either all of them or some of them depending on the mechanism of the process. On the other hand, too strong binding makes the reaction unfavorable and leads to a lower reaction rate. The third issue is that the newly formed adsorbate should be able to desorb from the surface or otherwise the reaction will lead to the formation of a passivation layer or to the poisoning of the surface that inhibits further catalysis. This principle is also known as the Sabatier's principle [1].

We have shown that by alloying it is possible to control the properties of transition metal surfaces. In principle this will allow one to determine which alloy should best suit for the desired purpose and to fabricate more efficient catalytic materials. Alloying Pd into an Ag surface promotes the CO oxidation into CO_2, which is an industrially crucial process. All the steps of the oxidation process, i.e. dissociation, adsorption and the reaction itself are related to the electronic structure of the adsorbates and the surface. Especially the center of the d-band and the d-band density of states at the Fermi-level are shown to correlate strongly with the reactivity of the surface.

Alloying Pd into Ag serves as a good model of the situation where a strong adsorbate in a more weakly binding surface promotes the catalysis. Basically the strength of the adsorption is determined by the center of d-band of the transition metal surface [29]. The surface must provide a channel for the mutual hybridization between the adsorbates to enable the reaction. This channel is formed via the hybridization of the electronic states of the adsorbate to the electronic states of the surface. For example, on clean Ag surface it is seen that there is no binding and no s-p hybridization, and therefore there will be no channel for charge transfer between the surface and the adsorbate.

Considering this, if we know the nature of bonding of adsorbates on an elemental transition metal surfaces, we can use this insight to think which kind of combination of materials would result to the most effective catalyst without testing all of the possible combinations. Up to this point we have considered only elemental surfaces and binary alloys, but the same principles are also applicable to more complex alloys. Perhaps the best catalytic surface for CO oxidation is still waiting to be found.

The *ab initio* methods have been found to be well suitable for catalytic studies. The controllable conditions and detailed information about the electronic structure and system energies allows us to do detailed analyis and to draw definite conclusions which helps understanding the underlying physics. For example, the method enables us to study the behavior and the role of the atomic orbitals during the adsorption and reaction processes. The *ab initio* calculations have been proven to be accurate in these problems, even though there exist several different kind of approximations of potentials and functionals. The absolute values of systems have some variation according to the chosen method, but especially the relative energies, such as adsorption and diffusion energies, are obtained consistently. The studies and results presented in this theses may be further extended to steps, strain and impurities to make the studies extensive and really applicable for drawing conclusions and deducting rules how the catalytic properties of surfaces behave.

The surface oxidation and the formation of reconstruction on Cu(100) have also been studied and it has been shown that the reconstructed surface is more inert to the adsorption and dissociation of O_2 than the unreconstructed Cu(100). Also, the diffusion of Cu and O adatoms on the reconstructed parts of the surface is significantly slower. This indicates that the reconstruction island growth at sub-monolayer O coverages is dominated by the dissociation of O_2 molecules and diffusion of O and Cu adatoms on the unreconstructed parts of the surface.

We have given an explanation to the formation of $c(2 \times 2)$-O domains based on the repulsive local interaction between the O adatoms. The formation of the domains seems to be purely a coverage driven process. A model based solely on the short range interactions explains experimentally observed results. This gives us a reason to believe that in this case the structures on the larger scales are caused by quantum mechanical short range interactions. These studies give new insight into the driving force behind the formation of the O covered domains. This far different ambiguous explanations for the domain formation have been suggested in the literature. The future extensions to the Cu oxidation studies are to take the gas phase oxygen into account and to extend the simulations into dynamical, non-equilibrium conditions.

In the multi-scale modeling, a larger scale model is based on the observations and results on a smaller scale. This serves as a controllable way to build a chain of models where one always knows what are the underlying

interactions. Combining *ab initio* studies with a larger scale model bridges the gap between the experiments and the electronic structure calculations. This is needed to be able to interpret further the experimental observations and to understand the underlying reasons for the emerged structures.

APPENDIX A: A Flow chart of the Monte Carlo code

In Fig. 16 we can see how the execution of the Monte Carlo simulation program flows. The basis of the program lies on three loops. The outmost loop includes different program runs and the initialization of the fundamental structures and data types. The next inner loop goes over the simulation time, hence over the number of Monte Carlo steps. All the observables are measured within this loop after a certain number of Monte Carlo steps. This conditioning may be bound to physics as well as straight to the number of steps. The number of steps in a simulation may be determined with a convergence criteria, according to coverage or with a fixed limit.

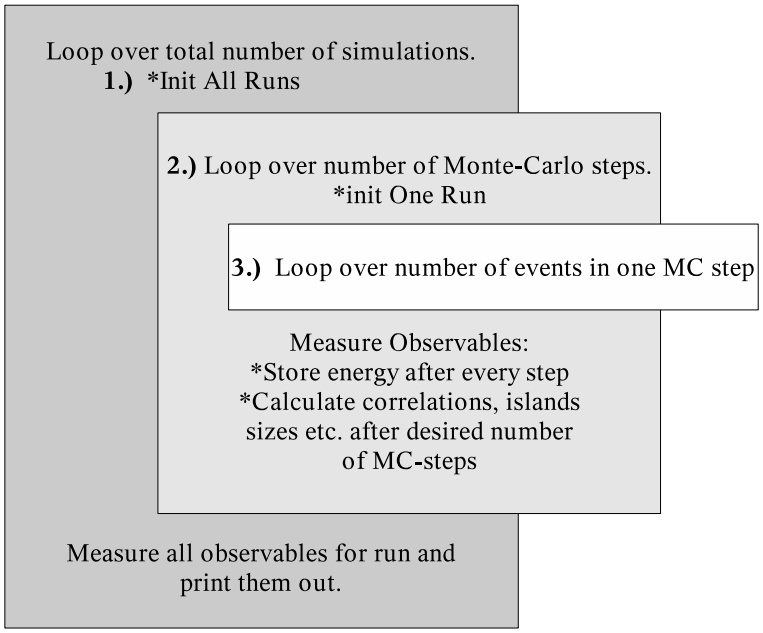

Figure 16: General flow chart of the program execution.

The innermost loop contains the elementary events in one Monte Carlo step. Within this loop an event is chosen and executed. Also the rates, configurations and search tree are updated after every single event.

References

[1] J. Hall, O. Saksager, and I. Chorkendorff. Dissociative chemisorption of O_2 on Cu(100). Effects of mechanical energy transfer and recoil. *Chem. Phys. Lett.*, 216:413, 1993.

[2] K.W. Kolasinski. *Surface science: Foundations of catalysis and nanoscience*. John Wiley & sons, LTD, 2002.

[3] H. Over, A. P. Seitsonen Y. D. Kim, E. Lundgren S. Wendt, M. Schmid, P. Varga, A. Morgante, and G. Ertl. Atomic-scale structure and catalytic reactivity of the $RuO_2(110)$ surface. *Science*, 287:1474, 2000.

[4] Kitco Bullion Dealers. *Kitco - Precious metals.* Kitco, http://www.kitco.com/, 2006.

[5] P.T. Wouda, M. Schmid, B.E. Nieuwenhuys, and P. Varga. STM study of the (111) and (100) surfaces of PdAg. *Surf. Sci.*, 417:292, 1998.

[6] M. Yata and H. Rouch. Control of the initial oxidation on Cu(001) surface by selection of translational energy of O_2 molecules. *Appl. Phys. Lett.*, 75:1021, 1999.

[7] M. Yata and Y. Uesugi-Saitow. Activated dissociation via a trapping precursor: O_2/Cu(001)$-(2\sqrt{2}\times\sqrt{2})$-O. *J. Chem. Phys*, 116:3075, 2002.

[8] P. Junell, M. Ahonen, M. Hirsimäki, and M. Valden. Influence of surface modification on the adsorption dynamics of O_2 on Cu(100). *Surf. Rev. Lett.*, 11:457, 2004.

[9] M. A. Van Daelen, M. Neurock, and R. A. van Santen. Reactivity of diatomic molecules on Cu(100). *Surf. Sci.*, 417:247, 1998.

[10] S. Stolbov and T.S. Rahman. Relationship between electronic and geometric structures of the O/Cu(001) system. *J. Chem. Phys.*, 117:8523, 2002.

[11] S. Stolbov, A. Kara, and T.S. Rahman. Electronic structure of the c(2×2)O/Cu(001) system. *Phys. Rev. B*, 66:245405, 2002.

[12] T.J. Stasevich, T.L. Einstein, and S. Stolbov. Extended lattice gas interactions of Cu on Cu(111) and Cu(001): Ab initio evaluation and implications. *Phys. Rev. B*, 73:115426, 2006.

[13] A. Bogicevic, S. Ovesson, P. Hyldgaard, B.I. Lundqvist, H. Brune, and D.R. Jennison. Nature, strength, and consequences of indirect adsorbate interactions on metals. *Phys. Rev. Lett.*, 85:1910, 2000.

[14] J. Rogal, K. Reuter, and M. Scheffler. CO oxidation at Pd(100): A first-principles constrained thermodynamics study. *arXiv:cond-mat*, page 0701777v1, 2007.

[15] K. Reuter and M. Scheffler. Composition and structure of the RuO_2 and CO environment: Implications for the catalytic formation of CO_2. *Phys. Rev. B*, 68:045407, 2003.

[16] T. Ohmi, A. Ohki, M. Nakamura, K. Kawada, T. Watanabe, Y. Nakagawa, S. Miyoshi, S. Takahashi, and M.S.K. Chen. The technology of chromium oxide passivation on stainless steel surface. *J. Electrochem. Soc.*, 140:1691, 1993.

[17] M. Kittel, M. Polcik, R. Terborg, J.-T. Hoeft, P. Baumgartel, A. M. Bradshaw, R. L. Toomes, J.-H. Kang, D. P. Woodruff, M. Pascal, C.L.A. Lamont, and E. Rotenberg. The structure of oxygen on Cu(100) at low and high coverages. *Surf. Sci.*, 470:311, 2001.

[18] B.C. Gates, J.R. Katzer, and G.C.A. Schuit. *Chemistry of catalytic processes*. McGraw-Hill Book Company, New York, 1979.

[19] N.W. Ashcroft and N.D. Mermin. *Solid State Physics*. Saunder College Publishing, Orlando, Florida, 1976.

[20] T. Kravchuk and A. Hoffman. Enhanced reactivity and selectivity in oxidation of Cu(100) and α-Cu-Al(5 at.%)(100) surfaces studied by electron and ion spectroscopies. *Surf. Sci.*, 600:1252, 2006.

[21] K. Reuter. Insight into a pressure and materials gap: CO oxidation at "ruthenium" catalysts. *Oil & Gas Science and Technology - Revue de l'IFP*, 61:471, 2006.

[22] A. Eichler. CO oxidation on transition metal surfaces: reaction rates from first principles. *Surf. Sci.*, 498:314, 2002.

[23] C. Stampfl and M. Scheffler. Density-functional study of the catalytic oxidation of CO over transition metal surfaces. *Surf. Sci.*, 433:119, 1999.

[24] C. Stampfl and M. Scheffler. Anomalous behavior of Ru for catalytic oxidation: A theoretical study of the catalytic reaction CO + $\frac{1}{2}$ O_2 → CO_2. *Phys. Rev. Lett.*, 78:1500, 1997.

[25] H.P. Kaukonen and R.M. Nieminen. Computer simulation studies of the catalytic oxidation of carbon monoxide on platinum surfaces. *J. Chem. Phys.*, 91:4380, 1989.

[26] A. Alavi, P. Hu, T. Deutsch, P.L. Silvestrelli, and J. Hutter. CO oxidation on Pt(111): An ab initio density functional theory study. *Phys. Rev. Lett.*, 80:3650, 1998.

[27] H.B. Gray. *Electrons and Chemical Bonding.* W.A. Benjamin, Inc, New Your, 1964.

[28] Axel Groß. *Theoretical Surface Science : A Microscopic Perspective.* Springer-Verlag, Berlin, 2002.

[29] B. Hammer and J.K. Nørskov. Electronic factors determining the reactivity of metal surfaces. *Surf. Sci.*, 343:211, 1995.

[30] G. Zheng and E.I. Altman. The oxidation of Pd(111). *Surf. Sci.*, 462:151, 2000.

[31] P. Hohenberg and W. Kohn. Inhomogenous electron gas. *Phys. Rev.*, 136:B864, 1964.

[32] R.M. Dreizler and E.K.U. Gross. *Density Functional Theory: An Approach to the Quantum Many-Body Problem.* Springer-Verlag, Berlin, 1990.

[33] W. Kohn and L.J. Sham. Self-consistent equations including exchange and correlation effects. *Phys. Rev.*, 140:A1133, 1965.

[34] R.O. Jones and O. Gunnarson. The density functional formalism, its applications and prospects. *Rev. Mod. Phys.*, 61:689, 1989.

[35] J. Perdew. Density-functional approximation for the correlation energy of the inhomogeneous electron gas. *Phys. Rev. B*, 33:8822, 1986.

[36] B. Hammer, L. B. Hansen, and J. K. Nørskov. Improved adsorption energetics within density-functional theory using revised Perdew-Burke-Ernzerhof functionals. *Phys. Rev. B*, 59:7413, 1999.

[37] J.A. White and D.M. Bird. Implementation of gradient-corrected exchange-correlation potentials in Car-Parrinello total-energy calculations. *Phys. Rev. B*, 50:4954, 1994.

[38] J.P. Perdew. Density-functional approximation for the correlation energy of the inhomogeneous electron gas. *Phys. Rev. B*, 33:8822, 1986.

[39] A.D. Becke. Density-functional exchange-energy approximation with correct asymptotic behavior. *Phys. Rev. A*, 38:3098, 1988.

[40] J.P. Perdew, K. Burke, and M. Ernzerhof. Generalized gradient approximation made simple. *Phys. Rev. Lett.*, 77:3865, 1996.

[41] W.E. Pickett. Pseudopotential methods in condensed matter applications. *Comm. Solid State Phys.*, 12:57, 1985.

[42] J. Callaway. *Energy Band Theory.* Academic Press, New York, 1964.

[43] J.C. Phillips and L. Kleinman. New method for calculating wave functions in crystals and molecules. *Phys. Rev.*, 116:287, 1959.

[44] D.R. Haman, M. Sclüter, and C. Chiang. Norm-conserving pseudopotentials. *Phys. Rev. Lett.*, 43:1494, 1979.

[45] D. Vanderbilt. Soft self-consistent pseudopotentials in generalized eigenvalue formalism. *Phys. Rev. B*, 41:7892, 1990.

[46] P.E. Blöchl. Projector augmented-wave method. *Phys. Rev. B*, 50:17953, 1994.

[47] G. Kresse. *Thesis.* Technische Universität, Wien, 1993.

[48] G. Kresse and J. Furthmuller. Efficiency of ab-initio total energy calculations for metals and semiconductors using a plane-wave basis set. *Comput. Mat. Sci.*, 6:15, 1996.

[49] G. Kresse and J. Furthmüller. Efficient iterative schemes for ab initio total-energy calculations using a plane-wave basis set. *Phys. Rev. B*, 54:11169, 1996.

[50] G. Kresse and J. Hafner. Ab initio molecular dynamics for liquid metals. *Phys. Rev. B*, 47:558, 1993.

[51] G. Kresse and J. Hafner. Norm-conserving and ultrasoft pseudopotentials for first-row and transition elements. *J. Phys.: Condens. Matter*, 6:8245, 1994.

[52] H.J. Monkhorst and J.D. Pack. Special points for Brillouinzone integrations. *Phys. Rev. B*, 13:5188, 1976.

[53] H. Ibach and H. Lüth. *Solid State Physics: An introduction to principles of materials science*. Springer, 1991.

[54] G. Kresse and J. Furthmüüller. *VASP the GUIDE*. Institut für Materialphysik, Universität Wien, http://cms.mpi.univie.ac.at/VASP/, 2005.

[55] G. Mills, H. Jónsson, and G. K. Schenter. Reversible work transition state theory: application to dissociative adsorption of hydrogen. *Surf. Sci.*, 324:305, 1995.

[56] H. Jónsson, G. Mills, and K. W. Jacobsen. *Nudged Elastic Band Method for Finding Minimum Energy Paths of Transitions', in 'Classical and Quantum Dynamics in Condensed Phase Simulations'*. World Scientific, 1998.

[57] J. Heinonen. *Diffusion and growth of steps and islands on surfaces*. PhD thesis, Helsinki University of Technology, 2000.

[58] M. Rusanen. *Island Growth and step instabilities on flat and vicinal surfaces*. PhD thesis, Helsinki University of technology, 2003.

[59] D. Landau and K. Binder. *A guide to Monte Carlo simulations in Statistical Physics*. Cambridge university press, Campridge, United Kingdom, 2000.

[60] P. Brémaud. *Markoc chains, Gibbs fields, Monte Carlo simulations and queues*. Springer Verlag, New York, 2001.

[61] C.P. Robert and G. Casella. *Monte Carlo statistical methods*. Springer Verlag, New York, 2002.

[62] N.G. Van Kampen. *Stochastic Processes in Chemistry and Physics*. North-Holland physics publishing, Amsterdam, 1981.

[63] D. Frenkel and B. Smit. *Understanding Molecular simulation : from algorithms to applications*. Academic press, 2002.

[64] L. E. Ballantine. *Quantum Mechanics: Modern development.* World Scientific, Singapore, 2001.

[65] N. Metropolis, A.W. Rosenbluth, A.H. Teller, and E. Teller. Equations of state calculations by fast computing machines. *Journal of Chemical Physics*, 21:1087, 1953.

[66] A.A. Bortz, M.H. Kalos, and J.L. Lebowitz. A new algorithm for monte carlo simulation of ising spin systems. *Journal of Computational Physics*, 17:10, 1975.

[67] J. Hoshen and R. Kopelman. Percolation and cluster distribution. I. cluster multiple labeling technique and critical concentration algorithm. *Phys. Rev. B*, 14:3438, 1976.

[68] J.L. Blue and I. Beichl. Faster Monte Carlo simulations. *Phys. Rev. E*, 51:R867, 1995.

[69] P.T. Wouda, M. Schmid, B.E. Nieuwenhuys, and P. Varga. Adsorbate migration on PdAg(111). *Surf. Sci. Lett.*, 423:229, 1999.

[70] B. Hammer, Y. Morikawa, and J.K. Nørskov. CO chemisorbtion at metal surfaces and overlays. *Phys. Rev. Lett.*, 76:2141, 1996.

[71] T. Vehviläinen, S. Jaatinen, and P. Salo. O_2 adsorption and dissociation on the Pd doped Ag surfaces: a density functional study. *Unpublished.*

[72] D. Butler, A. Raukema, and A. Kleyn. Molecular beam studies of the interaction of oxygen with silver surfaces. *J. Chem. Soc., Faraday Trans.*, 92:2319, 1996.

[73] P. Salo, K. Honkala, M. Alatalo, and K. Laasonen. Catalytic oxidation of CO on Pd(111). *Surf. Sci.*, 516:247, 2002.

[74] M. Alatalo, A. Puisto, H. Pitkänen, A.S. Foster, and K. Laasonen. Adsorption dynamics of O_2 on Cu(100). *Surf. Sci.*, 600:1574, 2006.

[75] T. Fujita, Y. Okawa, Y. Matsumotoa, and K. Tanaka. Phase boundaries of nanometer scale c(2×2)-O domains on the Cu(100) surface. *Phys. Rev. B*, 54:2167, 1996.

[76] A. Puisto, H. Pitkänen, M. Alatalo, S. Jaatinen, A.S. Foster, T. Kangas, and K. Laasonen. Adsorption of atomic and molecular oxygen on Cu(100). *Catal. Today*, 100:403, 2005.

[77] A. Soon, M. Todorova, B. Delley, and C. Stampfl1. Oxygen adsorption and stability of surface oxides on Cu(111) : A first-principles investigation. *Phys. Rev. B*, 73:165424, 2006.

[78] H. C. Zeng, R. A. McFarlane, and K. A. R. Mitchell. A LEED crystallographic investigation of some missing row models for the Cu(100)-$(2\sqrt{2} \times \sqrt{2})$ R45°-o surface structure. *Surf. Sci.*, 208:L7, 1988.

[79] G. Prévot, B. Croset, A. Coati, Y. Garreau, and Y. Girard. Self-organized systems for measuring surface stress at the nanoscale: N and O adsorption on Cu(001). *Phys. Rev. B*, 73:205418, 2006.

[80] I. Merrick, J.E. Inglesfield, and H. Ishida. Electronic structure and surface reconstruction of adsorbed oxygen on copper(001). *Surf. Sci.*, 551:158, 2004.